UNIVERSIDADE FEDERAL DO RIO GRANDE DO SUL
INSTITUTO DE FÍSICA
Programa de Pós-Graduação em Física

A fully kinetic model for the electron flow in a crossed field device

Samuel Marini

A thesis submitted in partial fulfillment of the requirements for the degree of Doctor of Philosophy in the Universidade Federal do Rio Grande do Sul-UFRGS.

Advisor: Dr. Renato Pakter - UFRGS
Co-Advisor: Dr. Felipe Barbedo Rizzato - UFRGS

Porto Alegre, RS
2016

to the love that keeps us together

Abstract

Using the kinetic description, a self-consistent model for the electron flow in the crossed electromagnetic field configuration observed in a smooth-bore magnetron was developed. Through that model, derived for both relativistic and nonrelativistic limit, it was possible to understand how the stationary states solutions for the electron flow change when the injection temperature, the charge intensity in the system, and the external electromagnetic fields were modified. Basing on the results, it was possible to characterize the regime transition (accelerating to space charge limited), the stability transition (laminar to turbulent flow) and the mode transitions (transitions between the modes: magnetic insulated, Child Langmuir, and non-cutoff). All the theoretical results were verified using self-consistent computer simulations.

Resumo

Nesse trabalho, utilizando a teoria cinética, desenvolveu-se um modelo auto-consistente para o fluxo de elétrons na configuração de campos eletromagnéticos cruzados observada em magnetrons planares. Através desse modelo, derivado tanto para o limite relativístico quanto para o limite não relativístico, pôde-se compreender como os estados estacionários do fluxo são afetados quando modifica-se a temperatura de injeção dos elétrons, a densidade de carga no sistema e os campos eletromagnéticos externos. Com base nos resultados obtidos, caracterizou-se a transição em que o fluxo de elétrons passa do regime acelerador para o regime desacelerador, a transição em que o fluxo de elétrons passa do estado laminar para o estado turbulento e, além disso, caracterizou-se as possiveis transições entre os modos estacionários confinado, parcialmente confinado e não confinado. Todos os resultados obtidos do modelo cinético foram comprovados através de simulações computacionais em que os campos eletromagnéticos auto-consistentes foram levados em conta.

Contents

Chapter 1

Introduction

This chapter gives a brief introduction to the work developed in this thesis.

1.1 State of the art

The electron dynamics description in a crossed electromagnetic field device is relevant to the development of several technological areas. Radar, electric thrusters, and linear accelerators have evolved with the upgrading of the theories and the models for this problem [1, 2, 3, 4]. Using the Newton's law for a single charged particle, Child [5], Hull [6], and Langmuir [7] published, at the beginning of the twentieth century, the first works describing the dynamics of a test electron in a crossed field configuration. In those works, only the external fields were taken into account. Nowadays, the theoretical description of the electron flow is more complex and, usually, in addition to the external electromagnetic fields, the self-fields are also taken into account [8, 9, 10, 11, 12, 13]. From those works, it is observed that the self-fields might be as relevant as the external fields. Nevertheless, due to the complexity that the self-fields add to the problem, in order to find the theoretical solutions the majority of the works assume the electron flow is cold [9, 10, 11, 14, 15, 16, 17] or is modeled by the fluid equations with a predetermined equation of state [12, 13].

Those assumptions might be inadequate in some special limits. Then, in this work, a kinetic mo-

del was developed to describe the electron dynamics, in special, the stationary states of the electron flow in a crossed electromagnetic field configuration like the one observed in a *smooth-bore magnetron*. The model was made taking into account the thermal effects and the self-fields together at the relativistic and the nonrelativistic limit. Moreover, a particle simulation to verify the theoretical solutions was run.

The *smooth-bore magnetron* is an approximation of the magnetron– an electromagnetic microwave generator used both in technological and ordinary devices, like radars and microwave ovens. Usually, a magnetron is composed of two concentric cylinders. The inner one is a cathode that emits electrons and the external one is an anode. The electrons emitted by the cathode rotate in the gap between the cylinders. In order to generate the microwaves, the anode has corrugates which produces small perturbations that accelerate and decelerate (a little bit) the electron flow. This acceleration/deceleration process is the mechanism that generates the electromagnetic waves. The magnetron's power can be raised by controlling and increasing the charge intensity in the gap. By control, it is understood to evaluate the electromagnetic fields that confine the electrons in the gap between the cylinders [1]. Here, to proceed with the evaluation of the electron confinement, firstly the corrugates were neglected and then the ratio between the inner and the external radius was supposed approximately the unity. When those conditions are satisfied, the planar shape of the smooth-bore magnetron is a good approximation of the real magnetron. Therefore, analyzing the smooth-bore magnetron, it is possible to determine the electron confinement and other important characteristics of the electron flow. A summary of the main results reported in this work is presented in the next section.

1.2 Thesis outline

The present work obeys the following organizational structure: in the beginning of Chapter 2, the theoretical model used to mathematically describe the smooth-bore magnetron is presented. To simplify the numeric results presentation, dimensionless quantities and parameters relevant to the

system are defined[1]. Assuming the electron flow initial momentum distribution is a *waterbag*, it is possible to show the charge density can be written as function of the position without knowing *a priori* where each electron is in the gap. From this finding, nonlinear equations to describe the stationary states of the flow at both relativistic and nonrelativistic limit are obtained. Moreover, in Chapter 2 the most relevant aspects of the particle simulation used here to verify the theoretical results are presented.

In Chapter 3 the main results obtained in this work are shown. The first analyzes are made supposing the electron flow is confined in the gap region and described by the nonrelativistic equations[2]. Fixing the injection temperature in a relatively small value and varying the charge intensity, it is verified that when the charge intensity goes to zero, the self-electric field is irrelevant and one stationary state governed by the external electric field is found. As the charge intensity is increased, the theory shows a region where multiple stationary state solutions are possible to the same charge intensity value. In that region, the electron flow could achieve the stationary state either being accelerated or decelerated (space charge limited regime) entering in the gap. However, the $N-$particle simulation indicates, in the multiple solutions region, the electron flow becomes stationary at the theoretically more accelerated expected solution (it means the flow is accelerated). Increasing even more the charge intensity, the multiple solutions region ceases, being replaced by a single decelerating stationary solution. The change between the multiple and the single solution region promotes an abrupt transition between the accelerate and the space charge limited regime.

Fixing the injection temperature in a relatively large value and varying the charge intensity, it is verified that the multiple solutions region disappears and, consequently, the abrupt mode transition does *not* occur. This indicates that there is a critical injection temperature which separates the abrupt and the continuous regime transitions. The theoretical critical injection temperature value is obtained through a parameter map. The results reported so far were obtained supposing the initial momentum distribution was a waterbag (uniform distribution) but it could be obtained supposing a more complex

[1] As the system, it is understood the physical structure with the electron flow.

[2] In the nonrelativistic limit, the self-magnetic field goes to zero and then, only the self-electric field is relevant. It simplifies obtaining both the theoretical and the computational results.

distribution, like a Gaussian, for example. The multiple solutions region had already been observed in the context of a cold plasma by Ref. [15], but nothing had been done for the thermal case. Therefore, the thermal results presented in this thesis are new and, differently from the cold case where the flow equations are linear, the thermal case results in complicated nonlinear equations, as it will be shown.

To observe the abrupt regime transitions, it is assumed that the electrons are pre-accelerated entering the gap. Although there are mechanisms to pre-accelerate the electrons (using lasers, for example [18]), it is more natural to assume the electrons are *not* pre-accelerated. It means there are electrons being emitted with velocities ranging from zero to large values, but the majority of the particles are emitted with velocities ranging from zero to a determined finite value. When there are electrons being emitted with zero initial velocity, it is found that the *final* steady state is modified due to intrinsic fluctuations of the charge density in the system. This result and the abrupt regime transition for the waterbag distribution were reported in an article published in the Physics of Plasmas [19] and the particular demonstration of the results validity assuming the initial Gaussian momentum distribution was reported in the Proceedings of IPAC15 [20].

Supposing the electrons are not pre-accelerated and the charge intensity in the gap is enough to shield the external electric field at the cathode (space charge limited regime), it is observed that at certain injection temperatures, the electron flow never becomes stationary. In order to understand this phenomenon, a theory based on an effective potential is developed. It is observed that the charge density oscillations prevent the electrons leaving the gap. Those electrons which become trapped in the gap oscillate indeterminately and, consequently, the flow can not achieve the steady state (it means the flow is turbulent). The charge density oscillations can destabilize the flow only when the charge intensity is large or when the injection temperature is small. It is also observed from the theory a turbulent region near the transition accelerator to decelerator but that region is small and could not be proved with the $N-$particle simulation due the precision required. To clarify for which parameters the flow does not become stationary, a parameter map is constructed. These results are new and they agree with the results for the cold case (which demonstrate the system never reaches the stationary state) showed in Ref. [15] and prove that the flow at the space charge limited regime presented in

Ref. [19] can[3] be at the stationary state. Recently these results were accepted to be published in the Physics of Plasmas [21].

The electron flow at the nonrelativistic limit when it is *not confined* (Child-Langmuir mode) is also analyzed in Chapter 3. At finite injection temperatures, it is found that the regime transition (accelerated to space charge limited) is followed by a mode transition *not confined* to *partially confined* (it means a mode transition from Child-Langmuir to no-cutoff). These transitions are continuous when the electrons are not pre-accelerated and occur abruptly whenever the electrons are pre-accelerated entering the gap. At the end of the nonrelativistic analysis, it is shown that the *partially confined* mode (no-cutoff mode) discussed in Ref. [12] can be treated, in the waterbag model, as a composition of *the confined* and the *not confined mode*. These latest results are unpublished and serve to understand how the parameter modify the electron flow.

At the end of Chapter 3, the main results obtained for the relativistic limit are presented. Specifically, the parameters (injection temperature and charge intensity) required to promote mode transitions when the flow becomes slightly relativistic are presented. It is observed that the mode transitions occurs due to variations in the self-magnetic field which modifies the magnetic shielding. Moreover, it is observed that when the injection temperature and the charge intensity go to zero, the electron flow is at the *partially confined* stationary state (no-cutoff mode) and increasing the injection temperature, it is possible to obtain a *confined* stationary solution (magnetic insulated mode). However, when the injection temperature is large enough, a *partially confined* solution emerge from the system again. Those results are also new since it was not found in any reference a kinetic model that takes into account the thermal and the self-fields effects simultaneously at the relativistic limit. Besides, it can be used to explain the reasons why there are always electrons reaching the anode, even when the common theories (which do not take into account the self-magnetic field and the thermal effects together at the relativistic limit) predicts electron confinement [22].

In Chapter 4 the conclusions which may be drawn from this thesis are presented and, at the Appendix A the solution for the scalar potential obtained using the Green's function method is shown.

[3] In a fact they are.

Chapter 2

Theoretical and computational approach

In this chapter, a theoretical model for the electron flow in a planar smooth-bore magnetron is presented, developed and analyzed. Besides, important details of the computer simulation used to verify the results from theory are described. At the end of the chapter, the nonrelativistic equation set is obtained as a limit of the relativistic case.

2.1 The physical model

The planar smooth-bore magnetron model that is analyzed in this work is presented in Fig. 2.1. There, two long parallel plates are kept at a constant potential difference. The plates are oriented in the $xz-$plane and separated by a distance L along the $y-$axis. The plate on $y = 0$ is a cathode kept at zero electric potential while the plate on $y = L$ is an anode kept at V_0 electric potential. As the consequence of the electric potential difference, there is a constant electric field $\mathbf{E}_0 = -(V_0/L)\hat{\mathbf{y}}$ in the region between the plates. Moreover, there is an external uniform constant magnetic field $\mathbf{B}_0 = -B_0\hat{\mathbf{z}}$ that is orthogonal to the electric field $\mathbf{E}_0$, consolidating the crossed-field configuration that is analyzed in this work.

Before the instant of time $t = t_0 = 0$, there is vacuum in the gap region between the plates ($0 < y < L$) but, at the instant of time t_0, the cathode starts emitting electrons that enter in the gap.

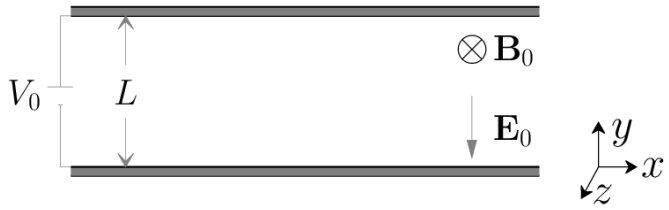

Fig. 2.1: Schematic model of a planar smooth-bore magnetron. In the figure, L and V_0 represent the distance and the potential difference between the cathode and the anode, respectively, and $\mathbf{E}_0$ and $\mathbf{B}_0$ are the electric and the magnetic field.

There, they are accelerated by the electric field $\mathbf{E}_0$ along the $y-$direction while they are deflected by the magnetic field $\mathbf{B}_0$ along the clockwise direction.

After a transient interval of time, an electron emitted by the cathode can reach the anode or return to the cathode. It depends on its initial velocity, the charge intensity in the gap, and the electromagnetic fields (external and the self-fields). Because electrons moving in the gap region generate self-electric $\mathbf{E}_s$ and self-magnetic $\mathbf{B}_s$ field, just to predict whether a particular electron will either reach the anode or return to the cathode is difficult but relevant to the industry. Thence, in the next sections, the mathematical and the computational model developed to determine the electron flow characteristics in crossed-field configurations are shown.

2.2 The basic relativistic equations

In this work, the kinetic theory is used to model the electron flow in the planar smooth-bore magnetron. In the absence of collisions, the time evolution of the electron distribution function in phase space $f = f(\mathbf{r}, \mathbf{P}, t)$ is given by the Vlasov equation

$$\frac{df(\mathbf{r}, \mathbf{P}, t)}{dt} = 0 \tag{2.1}$$

with the Maxwell equations:

$$\nabla \cdot \mathbf{E} = \frac{\rho}{\varepsilon_0}, \tag{2.2}$$

$$\nabla \cdot \mathbf{B} = 0, \tag{2.3}$$

$$\nabla \times \mathbf{E} = -\frac{\partial \mathbf{B}}{\partial t}, \tag{2.4}$$

and

$$\nabla \times \mathbf{B} = \mu_0 \left(\mathbf{J} + \varepsilon_0 \frac{\partial \mathbf{E}}{\partial t} \right), \tag{2.5}$$

where $\rho = -en$, with $n = \int f(\mathbf{r}, \mathbf{P}) d\mathbf{P}$ being the charge density, $\mathbf{J} = -en\mathbf{v}$ is the current density, $-e$ is the electron charge, $\mathbf{r}$ is the particle position, $\mathbf{P}$ is the particle canonical momentum, $\mathbf{v}$ is the particle velocity, and μ_0 and ε_0 are, respectively, the permittivity and the permeability of the free space [23].

Observing that the electromagnetic fields exhibit planar symmetry and assuming that the cathode emits large charge sheets in $xz-$plane, it is shown that the electron distribution function only depends on the $y-$coordinate. Therefore, Vlasov equation (2.1) can be written as follows:

$$\frac{\partial f}{\partial t} + \frac{\partial f}{\partial y}\frac{dy}{dt} + \frac{\partial f}{\partial P_y}\frac{dP_y}{dt} = 0. \tag{2.6}$$

Although it is assumed that the cathode emits large charge sheets instead of single electrons, here those are represented and treated like particles. The charge sheets supposition is usual [19, 20, 24, 25] and necessary to validate the unidimensional model.

According to the Hamiltonian formalism, the time evolution of the position and the canonical momentum along the $y-$coordinate are given by:

$$\frac{dy}{dt} = \frac{\partial H}{\partial P_y} \tag{2.7}$$

and:

$$\frac{dP_y}{dt} = -\frac{\partial H}{\partial y}, \tag{2.8}$$

where $H = H(\mathbf{r}, \mathbf{P}, t)$ is the single particle relativistic Hamiltonian. By using Eqs. (2.7) and (2.8), Eq. (2.6) can be rewritten as:

$$\frac{\partial f}{\partial t} + \frac{\partial f}{\partial y}\frac{\partial H}{\partial P_y} - \frac{\partial f}{\partial P_y}\frac{\partial H}{\partial y} = 0. \tag{2.9}$$

Thus, the evolution of the electron distribution function in phase space is described by Eq. (2.9). When $\partial f/\partial t = 0$, the flow becomes stationary.

The relativistic Hamiltonian for an electron (a charge sheet) in the planar smooth-bore magnetron can be written as:

$$H = c\sqrt{m^2c^2 + (\mathbf{P} + e\mathbf{A})^2} - e\phi, \tag{2.10}$$

where c is the speed of light, m is the electron rest mass, and ϕ and $\mathbf{A}$ are the scalar and the vector electromagnetic potentials [26]. It is worth to note that the electromagnetic potentials must reproduce the electromagnetic fields that satisfy the Maxwell equations. Given the following relation between the potentials and the electromagnetic fields [26]:

$$\mathbf{B} = \nabla \times \mathbf{A} \tag{2.11}$$

and

$$\mathbf{E} = -\nabla\phi - \frac{\partial \mathbf{A}}{\partial t}, \tag{2.12}$$

it is possible to verify that Maxwell equations (2.3) and (2.4) are satisfied. Moreover, supposing the

electrostatic case (the potentials constant in time) and using the relation (2.12) in (2.2), the Poisson equation for the scalar potential as function of the particle density is obtained, such that:

$$-\frac{\partial^2\phi}{\partial y^2} = -\frac{e}{\varepsilon_0}n(y), \tag{2.13}$$

where it was used that the particle density only depends on $y-$spatial coordinate. Eq. (2.13) must satisfy the following boundary conditions:

$$\phi(y=0) = 0 \tag{2.14}$$

and

$$\phi(y=L) = V_0. \tag{2.15}$$

The boundary conditions (2.14) and (2.15) refer to the scalar potential over the cathode and the anode, respectively. When there is *no* charge in the gap, Eq. (2.13) with the boundary conditions reproduce the external scalar potential, consequently, the external electric field. However, as charges enter the system, the scalar potential is modified such as the electric field become the superposition of the external and the self-electric field.

Finally, supposing the electrostatic case and using the relation (2.11) in (2.5), a differential equation for the vector potential is obtained[1]. In this model, the electrons start moving along the $y-$direction but due to the external magnetic field, they are accelerated especially along the $x-$direction. It sets $\mathbf{A} = A_x(y)\hat{\mathbf{x}}$. Consequently, the potential vector can be determined by the following equation:

$$-\frac{\partial^2 A_x}{\partial y^2} = \mu_0 J_x(y), \tag{2.16}$$

where $J_x(y) = -ev_x(y)n(y)$ is the x component of the current density. Eq. (2.16) must satisfy the following boundary conditions:

[1]It was also used the mathematical relation $\nabla \times \nabla \times \mathbf{A} = \nabla(\nabla \cdot \mathbf{A}) - \nabla^2\mathbf{A}$ and the Coulomb gauge $\nabla \cdot \mathbf{A} = 0$.

$$A_x(y=0)=0 \tag{2.17}$$

and

$$\frac{\partial A_x}{\partial y}\Big|_{(y=L)} = -B_0. \tag{2.18}$$

The potential vector value at cathode could be any constant but to ensure that the kinetic momentum ($\mathbf{p} = \mathbf{P} + e\mathbf{A}$) is equal to the canonical momentum of the particles at emission and that the particles have only velocity along the $y-$direction (the electrons do not slip over the cathode), the condition (2.17) is used. Moreover, it is assumed that, experimentally, the measure of the magnetic field is made over the anode and results at $-B_0$ value. As a consequence, the boundary condition (2.18) was written. Note, there is *not* any information about the magnetic field measured over the cathode when there are particles in the magnetron. Indeed, the particles moving in the gap produce a self-magnetic field that decreases the magnetic field measured at the cathode.

Summarizing, to describe the steady states of the electron flow in the crossed-field configuration, it is necessary to solve the Hamiltonian given by Eq. (2.10) where the electromagnetic potentials are given by (2.13) and (2.16) [23, 26].

2.2.1 Dimensionless quantities

In this section, dimensionless quantities based on the physical model of the planar smooth-bore magnetron are defined. The dimensionless quantities are useful because they can simplify the basic equation set. Since the cathode-anode distance is L (see Fig. 2.1), it is convenient to define a dimensionless coordinate, such as:

$$\tilde{y} \equiv \frac{y}{L}. \tag{2.19}$$

It is also convenient to define a dimensionless canonical momentum:

$$\tilde{\mathbf{P}} \equiv \frac{1}{\Omega_c m L}\mathbf{P}, \tag{2.20}$$

where $\Omega_c = eB_0/m$ is the cyclotron frequency. Additionally, a dimensionless electron velocity

$$\tilde{\mathbf{v}} \equiv \frac{1}{\Omega_c L}\mathbf{v}, \tag{2.21}$$

a dimensionless energy

$$\tilde{H} \equiv \frac{1}{\Omega_c^2 m L^2}H, \tag{2.22}$$

a dimensionless scalar potential

$$\tilde{\phi} \equiv \frac{1}{V_0}\phi, \tag{2.23}$$

and a dimensionless vector potential

$$\tilde{A}_x \equiv \frac{1}{B_0 L}A_x \tag{2.24}$$

are defined. From this point on, these dimensionless quantities will be used but the superscript tilde will be suppressed. Now, using the dimensionless quantities (2.19), (2.20) and (2.22)−(2.24), it is possible to write the dimensionless Hamiltonian

$$H = \frac{\nu_0}{2\zeta_0}\sqrt{1 + \frac{2\zeta_0}{\nu_0}\left((P_x + A_x)^2 + P_y^2 + P_z^2\right)} - \frac{\nu_0}{2}\phi(y). \tag{2.25}$$

where the dimensionless parameters

$$\zeta_0 = \frac{eV_0}{mc^2} \tag{2.26}$$

and

$$\nu_0 = \frac{V_0}{V_H}, \tag{2.27}$$

presented in Eq. (2.25) were defined as the relativistic parameter and the accelerating potential. The relativistic parameter ζ_0 measures how important are the relativistic effects. When ζ_0 goes to zero, the system becomes described by the nonrelativistic equations. In Eq. (2.27), $V_H = eB_0^2L^2/2m$ is the Hull potential [6]. In a nonrelativistic system, the Hull potential is the potential necessary to accelerate an electron emitted from the cathode with zero velocity until it reaches the anode with the same (zero) velocity. Therefore, when $\nu_0 = 1$ an electron emitted from the cathode with zero velocity will reach the anode with the same zero velocity.

The Hamiltonian given by (2.25) does *not* depend explicitly on variables x and z. Therefore, the canonical momenta P_x and P_z are constants of motion and their values are determined by the electron velocity entering the gap region. To simplify the analysis, it is assumed that the electrons are emitted with orthogonal velocity to the cathode, such as $P_x = 0$ and $P_z = 0$. However, it should be noted, it does *not* imply that the velocity parallel to the cathode is zero[2], indeed: $\mathbf{v}_\parallel = (\mathbf{P}_\parallel + \mathbf{A}_\parallel)/\sqrt{1 + 2\zeta_0(\mathbf{P} + \mathbf{A})^2/\nu_0}$. Consequently, the $\hat{\mathbf{x}}$ component of the velocity is given by:

$$v_x(y) = \frac{A_x(y)}{\sqrt{1 + \frac{2\zeta_0}{\nu_0}(A_x^2(y) + P_y^2)}}. \tag{2.28}$$

The potentials in Hamiltonian equation (2.25) are dimensionless, therefore, it is necessary to find the normalized equations that describe those. Using definitions (2.19), (2.23) and

$$\tilde{n} \equiv \frac{n}{n_0}, \tag{2.29}$$

where n_0 is the electron density over the cathode, it is possible to write the Poisson equation (2.13) as:

[2]To ensure the no-slip condition over the cathode, it is necessary to use $A_x(0) = 0$. That justifies the bondary condition presented in Eq. (2.17).

$$\frac{\partial^2 \phi}{\partial y^2} = \eta_0 n(y). \tag{2.30}$$

The scalar potential (2.30) must satisfy the dimensionless boundary conditions:

$$\phi(0) = 0 \tag{2.31}$$

and

$$\phi(1) = 1. \tag{2.32}$$

The parameter η_0 is the charge intensity defined as:

$$\eta_0 = \frac{e n_0 L^2}{\varepsilon_0 V_0}. \tag{2.33}$$

The charge intensity is a measure of the charge importance in the gap. It means when $\eta_0 = 0$ the charge in the gap is not important and, consequently, the self-fields are null. Using definitions (2.19), (2.21), (2.24), (2.26), and (2.33), it is possible to write an equation for the vector potential (2.16) as:

$$\frac{\partial^2 A_x}{\partial y^2} = \eta_0 \zeta_0 v_x(y) n(y) \tag{2.34}$$

satisfying the following normalized boundary conditions:

$$A_x(0) = 0 \tag{2.35}$$

and

$$\left.\frac{\partial A_x}{\partial y}\right|_{(y=1)} = -1. \tag{2.36}$$

2.2.2 The initial charge distribution and the waterbag model

In this model, it is assumed that the electrons are emitted from the cathode ($y = 0$) with an initial canonical momentum that is distributed according to a waterbag distribution. Thereby, the electrons

can be emitted with any initial canonical momentum value within a range defined by a minimum (P_{0min}) and a maximum (P_{0max}) value. The waterbag distribution was adopted because series of waterbag can recreate other function distributions [27, 28] and, in this case, it can reproduce results obtained by using a more complex function, like a Gaussian distribution [20] (it will be shown in Chapter 3).

Explicitly, the waterbag electron canonical momentum distribution on the cathode is given by:

$$f(P_y, y=0) = \begin{cases} \frac{1}{P_{0max}-P_{0min}} & \text{if} \quad P_{0min} \leq P_y \leq P_{0max}, \\ 0 & \text{if} \quad P_y < P_{0min} \qquad \text{and} \qquad P_y > P_{0max}, \end{cases} \tag{2.37}$$

Observing that the convective derivative of $f(y, P_y, t)$ vanishes according to Vlasov equation, the flow evolves over the phase space as an incompressible fluid and, therefore, the density at any point in phase space must be the same. Then, multiplying the initial density ($1/(P_{0max} - P_{0min})$) by the area occupied by the electron flow in the phase space results in the electron density as function of position. The area occupied by the electron flow in the phase space depends on the trajectory of the most and the least energetic electrons of the distribution at the stationary mode (to clarify, see the solid lines in Fig. 3.2). To the waterbag initial canonical momentum distribution of particles, three stationary modes are possible [12], they are: *magnetic insulation*, *Child-Langmuir*, and *no-cutoff mode*. The *magnetic insulation (MI) mode* occurs when all electrons emitted from the cathode return to it after a transient time. In that stationary mode, the electron density as function of the coordinate can be written as:

$$n_{MI}(y) = 2\frac{|P_y(P_{0max}, y)| - |P_y(P_{0min}, y)|}{P_{0max} - P_{0min}}, \tag{2.38}$$

where $P_y(P_{0max}, y)$ and $P_y(P_{0min}, y)$ are the canonical momentum as a function of the coordinate y for the most and the least energetic electrons. The canonical momentum equation is obtained observing that the equality $H(y = 0) = H(y)$ for $0 \leq y \leq 1$ is true at stationary state since the system is conservative. Then, from the Hamiltonian (2.25), it is obtained:

$$P_y(P_0, y) = \pm\sqrt{P_0^2 - A_x^2(y) + \phi(y)\sqrt{\nu_0\left(\nu_0 + 2P_0^2\zeta_0\right)} + \frac{1}{2}\nu_0\zeta_0\phi^2(y)}, \tag{2.39}$$

where P_0 is the canonical momentum of the electron at the cathode and the plus (minus) sign refers to electrons moving toward the anode (cathode). The canonical momentum (2.39) is a real function to be considered zero whenever it becomes imaginary. Supposing $P_y(P_{0max}, y = 1) = 0$ (the first electron that can reach the anode) in Eq. (2.39), it is possible to conclude that the MI mode occurs when

$$\nu_0 = \nu_{MI} < \frac{2\left(A_x^2(y=1) + P_{0max}^2\right)\zeta_0 - 4\sqrt{\left(A_x^2(y=1) - P_{0max}^2\right)^2 + A_x^2(y=1)P_{0max}^2\zeta_0^2}}{\zeta_0^2 - 4}, \tag{2.40}$$

where $A_x(y = 1)$ is the vector potential evaluated on the anode. It depends on the electron distribution in the gap region such as, when only the external magnetic field is taken into account, $A_x(y = 1) = -1$.

The *Child-Langmuir (CL) mode* occurs when all electrons emitted from the cathode reach the anode after a transient time. In that stationary mode, the electron density as function of the coordinate is:

$$n_{CL}(y) = \frac{|P_y(P_{0max}, y)| - |P_y(P_{0min}, y)|}{P_{0max} - P_{0min}}. \tag{2.41}$$

Differently from Eq. (2.38), in Eq. (2.41) the numerical factor "2" does not appear. This occurs because in the MI mode the electrons are going to the anode and returning to the cathode while in the CL mode they are just going to the anode. Supposing $P_y(P_{0min}, y = 1) = 0$ in Eq. (2.39) (This is equivalent to assume that the less energetic electron reaches the anode), it is possible to observe that the condition for the emergence of the CL mode is:

$$\nu_0 = \nu_{CL} > \frac{2\left(A_x^2(y=1) + P_{0min}^2\right)\zeta_0 - 4\sqrt{\left(A_x^2(y=1) - P_{0min}^2\right)^2 + A_x^2(y=1)P_{0min}^2\zeta_0^2}}{\zeta_0^2 - 4}. \quad (2.42)$$

Finally, the *no-cutoff (NC) mode* occurs when part of the electrons reach the anode and part of electrons return to the cathode. In that stationary mode, the electrons emitted from the cathode with momentum ranging from P_{0min} to below P_{0lim} return to it after a transient time and so the mathematical treatment of those electrons is equal to the MI mode. In addition, the electrons with momentum from P_{0lim} to P_{0max} reach the anode and so the mathematical treatment of those electrons is equal to the CL mode. Here, P_{0lim} is defined as the initial canonical momentum of the less energetic electron which reaches the anode, satisfying the condition $P_{0min} \leq P_{0lim} \leq P_{0max}$, such as:

$$P_{0lim} = \sqrt{A_x^2(y=1) + P_y^2(P_{0lim}, y=1) + (\nu_0\zeta_0)/2 - \sqrt{\nu_0^2 + 2\nu_0\zeta_0 A_x^2(y=1) + \zeta_0 P_y^2(P_{0lim}, y=1)}}, \quad (2.43)$$

where $P_y(P_{0lim}, y=1)$ is the electron momentum of the first electron which arrives to the anode. Thus, the electron density as function of position at NC mode can be written as follows:

$$n_{NC}(y) = 2\frac{|P_y(P_{0lim}, y)| - |P_y(P_{0min}, y)|}{P_{0max} - P_{0min}} + \frac{|P_y(P_{0max}, y)| - |P_y(P_{0lim}, y)|}{P_{0max} - P_{0min}}. \quad (2.44)$$

The first term of Eq. (2.44) refers to the electrons which return to the cathode while the second term refers to the electrons which reach the anode. Combining the restrictions of the MI and the NC modes, it is possible to observe that the NC mode occurs when $\nu_{MI} < \nu_0 \leq \nu_{CL}$.

For a parameter set ν_0, η_0, ζ_0 and initial momentum distribution, the stationary mode of the flow is inferred and the electron density is given by either (2.38), (2.41) or (2.44). Then, the electromagnetic potentials are obtained by using the selected electron density in Eqs. (2.30) and (2.34). Later, the

dynamics of the faster and the lower electron of the momentum distribution in phase space (Eq. (2.39)) are evaluated using the electromagnetic potentials. The final result validates or discards the assertion made about the electron density. If it is discarded, the process is restarted. The results obtained from this theoretical approach are presented and compared with the results from particle simulation in Chapter 3.

Since the equations for the potentials are nonlinear, it is hard (or impossible) to obtain an analytic solution. So, an adaptive Sixth-order Runge-Kutta integrator to solve them numerically [29] was used. In practice, the potentials were solved as an initial value problem by setting the boundaries $\phi(0) = 0$ and $A_x(0) = 0$ and taking a guess value for the electric (E_c) and the magnetic field at the cathode (B_c). Then, using the Newton-Raphson Method [29], a value for E_c and B_c that satisfies the correct boundary condition at the anode $\phi(1) = 1$ and $\partial A_x/\partial y|_{y=1} = -1$ was found.

Now, it is appropriate to define two more dimensionless parameters: the average electron momentum and the injection temperature. The average electron momentum is defined as:

$$\bar{P_0} = \frac{\int f(P_y, y = 0) P_y dP_y}{\int f(P_y, y = 0) dP_y}. \tag{2.45}$$

Using the waterbag distribution, the average electron momentum at emission can be written as:

$$\bar{P_0} = \frac{P_{0max} + P_{0min}}{2}. \tag{2.46}$$

The dimensionless injection temperature is defined as follow:

$$T_0 = \frac{\int f(P_y, y = 0) P_y^2 dP_y}{\int f(P_y, y = 0) dP_y} - \bar{P}_0^2. \tag{2.47}$$

Specifically, to the waterbag distribution, it is found:

$$T_0 = \frac{(P_{0max} - P_{0min})^2}{12}. \tag{2.48}$$

Observe that T_0 is a measure of the electron momentum spread around the average electron mo-

mentum at injection supposing the Boltzmann constant equal to the unity [24]. From definition (2.46) and (2.48), it can be found that: $P_{0max} = \bar{P}_0 + \sqrt{3T_0}$ and $P_{0min} = \bar{P}_0 - \sqrt{3T_0}$.

2.3 Relevant aspects of the computational model

In order to verify the assumptions used to obtain the theoretical solutions, a self-consistent computer simulation was run. In the simulation, N particles are emitted from the cathode with a given initial momentum distribution. The position evolution of the ith electron can be derived from the Hamiltonian described in Eq. (2.25) resulting in:

$$\frac{dy_i}{dt} = \frac{P_y^i}{\sqrt{1 + \frac{2\zeta_0}{\nu_0}\left((P_y^i)^2 + A_x^2\right)}}, \tag{2.49}$$

where $1 \leq i \leq N$ is the electron label. Complementarily, the canonical momentum evolution is given by:

$$\frac{dP_y^i}{dt} = -\frac{\nu_0}{2}E_y^i - \frac{A_x B_z}{\sqrt{1 + \frac{2\zeta_0}{\nu_0}\left((P_y^i)^2 + A_x^2\right)}}, \tag{2.50}$$

where the time in Eqs. (2.49) and (2.50) is normalized by Ω_c. The electric field can be evaluated from Eq. (2.30) with the boundary conditions (2.31) and (2.32), using the Green's function method [24, 30] (see appendix A) outcome in:

$$E_y^i = -\left(1 + \eta_0\bar{y} - \eta_0\frac{n_r^i}{N}\right), \tag{2.51}$$

where $\bar{y} \equiv \frac{1}{N}\sum_{i=1}^{N} y_i$ is the electron average position, $n_r^i \equiv N - i + 1$ is the number of electrons above the ith electron plus one and N is the total number of electrons in the gap. On the other hand, there is not a simple solution for the magnetic field, then, it is calculated by using an electrostatic particle-in-cell (PIC) method[3] [31]. In fact, it was used the Thomas algorithm to solve the equation

[3]Here it is called particle-in-cell because de the particle density was evaluated over small cells.

for the vector potential (2.34) with boundaries. In order to use the Thomas algorithm, the right side of the (2.34) was given in a instant of time before to proceed with the evaluation of the differential equation. Through this procedure, the second order differential equation (2.34) could be treated like a linear equation. When the variations of the vector potential are small, that approximation is true [29].

In order to recreate a real device in the simulation, it is assumed that when $t < t_0$, there is vacuum in the gap region between the cathode and the anode. However, at the instant of time t_0, electrons start being emitted from the cathode ($y = 0$) with initial momentum determined by a waterbag distribution (it will be also used a Gaussian initial distribution, see subsection 3.1.2). The dynamics of each electron is given by Eqs. (2.49) and (2.50). When an electron reaches the anode or returns to the cathode, it is removed from the simulation. Particularly to the waterbag distribution, the number of electrons entering in the simulation keeps the density in the phase space constant and uniform. Thus, it changes according to the phase space area. In the simulations made to this work, the number of electrons in the gap region is approximately[4] 10000.

Through simulation, the time evolution of the electric $E_c(t)$ and the magnetic field $B_c(t)$ at the cathode is measured. After a transient period of time, the fields become time independent. When this happens, it is assumed that the flow is at the stationary state.

2.4 The nonrelativistic limit

Since the nonrelativistic case is more simple and has many applications, it will be exhaustively analyzed in the chapter of the results (Chapter 3). To clarify which are the equations used there, the nonrelativistic equations are derived here as a limit of the relativistic case. In the nonrelativistic approach, the relativistic parameter and the self-magnetic field go to zero. Consequently, the particle Hamiltonian becomes described by the classical equations of motion and the magnetic field described by the external magnetic field. It simplifies the obtention of the theoretical and computational results.

Because the relativistic parameter goes to zero ($\zeta_0 \to 0$), it is possible to use the Taylor series of

[4] In a special case to verify the flow stability a large number of particles was used (about 90000).

square root in the relativistic Hamiltonian equation (2.25), resulting in:

$$H = \frac{\nu_0}{2\zeta_0}\left(1 + \frac{1}{2}\left(P_y^2 + A_x^2(y)\right)\frac{2\zeta_0}{\nu_0}\right) - \frac{\nu_0}{2}\phi(y), \tag{2.52}$$

where the result $P_x = P_z = 0$ has been used. Observing that $\nu_0/2\zeta_0$ is a constant and defining, without loss of generality, the nonrelativistic Hamiltonian $H_c \equiv H - \nu_0/2\zeta_0$, it is found:

$$H_c = \frac{P_y^2}{2} + \frac{A_x^2(y)}{2} - \frac{\nu_0}{2}\phi(y). \tag{2.53}$$

Although Eq. (2.53) was derived from the single particle relativistic Hamiltonian, it could be derived from the classical formulation, resulting as the same. Moreover, it is possible to observe that the equation for the vector potential (2.34) with the boundary conditions can be solved when the nonrelativistic condition $\zeta_0 \to 0$ is used, resulting in:

$$A_x(y) = -y. \tag{2.54}$$

It means the self-magnetic field goes to zero in the nonrelativistic approach. Using the result (2.54) in the Hamiltonian (2.53) and assuming $H_c(0) = H_c(y)$, the following equation for the canonical momentum is obtained:

$$P_y(P_0, y) = \pm\sqrt{P_0^2 - y^2 + \nu_0\phi(y)}. \tag{2.55}$$

The scalar potential equation does not depend on ζ_0, then the same equation used to describe the scalar potential in the relativistic case (2.30) is used here to describe the nonrelativistic case. However, the canonical momentum function used to describe the electron density must be replaced by Eq. (2.55). In order to clarify, supposing the MI mode[5], the scalar potential equation to be solved is:

[5]To the MI mode, the particle density is given by Eq. (2.38).

$$\frac{\partial^2\phi}{\partial y^2} = 2\eta_0 \frac{|\sqrt{P_{0max}^2 - y^2 + \nu_0\phi(y)}| - |\sqrt{P_{0min}^2 - y^2 + \nu_0\phi(y)}|}{P_{0max} - P_{0min}}, \tag{2.56}$$

subject to the boundaries $\phi(0) = 0$ and $\phi(1) = 1$. Note that, even in the classical case, the equation for the scalar potential (2.56) is nonlinear and a numerical method is necessary to solve it. Once the potential equation is solved, the classical Hamiltonian (2.53) becomes completely defined and then, it is possible to get theoretical information about the trajectory of any particle in the system.

Finally, using the nonrelativistic approximation in Eq. (2.49) used in the simulation to describe the electron position evolution, the following equation is found:

$$\frac{dy_i}{dt} = P_y^i, \tag{2.57}$$

where $1 \leq i \leq N$ is the electron label. Complementarily, using the nonrelativistic approximation in Eq. (2.50) used in the simulation to describe the electron momentum evolution, the following equation is obtained:

$$\frac{dP_y^i}{dt} = -\frac{\nu_0}{2} E_y^i - y_i, \tag{2.58}$$

where the result (2.54) for the vector potential was used and the electric field E_y^i is still given by Eq. (2.51). As it was anticipated, the equations derived in this section will be employed in the chapter of results to describe the electron flow in the nonrelativistic approximation.

Chapter 3

Results

In this chapter, the results obtained for the electron flow in the crossed-field configuration are shown for both relativistic and nonrelativistic approach. Firstly, the results from the nonrelativistic approach are presented and analyzed and then, at the end of this chapter, they are extended to the relativistic limit.

3.1 Nonrelativistic magnetic insulation mode

Here, using the nonrelativistic equation set obtained in section 2.4, the magnetic insulation mode is analyzed. In the MI mode, all electrons emitted by the cathode return to it after a transient time and the scalar potential is given by Eq. (2.56) with the boundary conditions. Solving the scalar potential equation (Poisson equation), it is possible to describe all the electron trajectories in the phase space as well as to evaluate the electric field at the cathode $E_c = -\partial\phi/\partial y|_{y=0}$. The E_c value is important because it identifies whether the electrons are accelerated or decelerated (space charge limited regime) entering in the gap region. Using $\zeta_0 = 0$ and Eq. (2.54) in Eq. (2.40), it is possible to observe that the MI mode occurs when the condition

$$\nu_0 < 1 - P_{0max}^2 \tag{3.1}$$

is true.

3.1.1 Continuous and abrupt regime transitions

The results from the theory (solid line) and from the simulation (points) for the normalized electric field E_c/E_0 as a function of the charge intensity using $\nu_0 = 0.8$ (MI mode), $\bar{P}_0 = 0.2$ and $T_0 = 8.33 \times 10^{-4}$ are shown in Fig. 3.1(a). When $\eta_0 \to 0$, the scalar potential approaches the vacuum solution $\phi(y) = y$ and, consequently, $E_c = E_0 = -1$. As the charge intensity increases, the normalized electric field decreases. It does occur because progressively more and more charges are present in the gap region and that shield the external electric field. When $\eta_0 \approx 0.836$, the charge intensity in gap region is large enough to shield the external electric field at the cathode and a single stationary solution that corresponds to the space charge limited regime ($E_c/E_0 < 0$) is found. When $\eta_0 < 0.820$ or $\eta_0 > 0.835$, there is only one stationary solution for the electron flow. However, when $0.820 < \eta_0 < 0.835$ there are three different solutions, indicating that the electron flow can change from one to another solution branch with the same η_0.

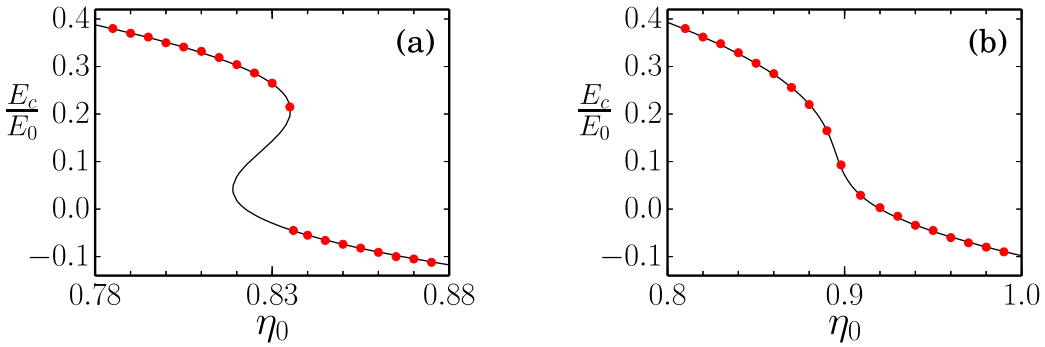

Fig. 3.1: Normalized electric field at the cathode for the stationary state as function of the charge intensity η_0 for (a) $T_0 = 8.33 \times 10^{-4}$ and (b) $T_0 = 3.33 \times 10^{-3}$. The solid line corresponds to results from the theory, whereas the symbols from the simulation. Accelerating and space charge limited regime correspond to $E_c/E_0 > 0$ and $E_c/E_0 < 0$, respectively. Other parameters are $\nu_0 = 0.8$ (magnetic insulation mode) and $\bar{P}_0 = 0.2$.

This scenario was verified by a $N-$particle simulation (points in Fig. 3.1) and a very good agreement with the theory was observed. Particularly, in the multiple solutions region, the results from

simulation follow the upper (more accelerate) branch. However, as the charge intensity is increased, the multiple solutions region ceases and the system jumps from the accelerating ($E_c/E_0 = 0.2$) to the space charge limited regime ($E_c/E_0 = -0.05$), characterizing transition that is similar to a nonequilibrium[1] first order phase transition [32, 33].

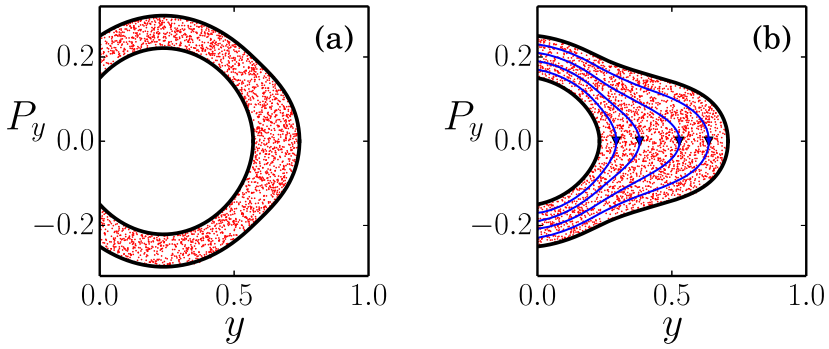

Fig. 3.2: Phase space plots of the stationary state in the vicinity of the abrupt regime transition. Dots are the particle position in phase space obtained from simulation after the flow became stationary and thick black lines correspond to the charge distribution boundaries predicted by the theory. A slight change in the charge intensity from (a) $\eta_0 = 0.835$ to (b) $\eta_0 = 0.836$ drives the system from the accelerating to the space charge limited regime, producing a dramatic change in the charge distribution. Thin blue curves in (b) represent four real trajectories obtained from the simulation, showing that the electron flow is laminar.

In order to visualize the abrupt regime transition, the electron flow phase space at stationary state before and after the abrupt regime transition were plotted in Fig. 3.2. When $\eta_0 = 0.835$ the electron flow is accelerated entering the gap region as is shown in Fig. 3.2(a), in opposition, when the charge intensity is increased slightly greater to $\eta_0 = 0.836$, the electron flow is decelerated entering the gap region as is shown in Fig. 3.2(b). In that figures, black lines are the results from theory for the most ($P_y(P_{0max}, y)$) and the least ($P_y(P_{0min}, y)$) energetic electrons and dots are the particle position in the phase space obtained from simulation after the flow became stationary. It is possible to observe the theoretical solutions describe very well the results obtained from the simulation for the electron flow.

The blue lines in Fig. 3.2(b) were obtained from $N-$particle simulation and they show four real electron trajectories since the emission until the absorption. Analyzing that curves, it is observed

[1] It because the collisions are neglected.

that the electron flow is laminar[2], even at the space charge limited regime. The laminar condition is necessary to validate the theoretical analysis and to confirm the flow is at a true stationary state.

The results from the theory (solid line) and from the simulation (points) for the normalized electric field E_c/E_0 as function of charge intensity are shown in Fig. 3.1(b). There, the parameters are the same used in Fig. 3.1(a), except the temperature which was increased to $T_0 = 3.33 \times 10^{-3}$. In contrast to the results of Fig. 3.1(a), now the theory predicts only a single stationary solution branch. Consequently, the transition between accelerating and decelerating regime is continuous. The prediction is confirmed noting the results from simulation (points) agree with the results from theory (solid line).

3.1.2 Gaussian initial momentum distribution

Although the theory of the electron flow in the crossed-field configuration developed here was based on the waterbag initial momentum distribution, it can predict results which are obtained by using a more complex distribution, like the Gaussian initial momentum distribution [20]. Thereby, the curves presented in Figs. 3.1 and 3.2 were redrawn in order to include the results obtained from the computer simulation supposing the following Gaussian initial momentum distribution:

$$f_g(P_y, y=0) = \begin{cases} \frac{1}{\sqrt{2\pi T_0^2}} e^{-\frac{(P_y-\bar{P}_0)^2}{2T_0^2}} & \text{if} \quad \bar{P}_0 \geq 0, \\ 0 & \text{if} \quad \bar{P}_0 < 0, \end{cases} \tag{3.2}$$

where T_0 used here is the same presented in Eq. (2.47). The parameters used in Fig. 3.1 was also used in Fig. 3.3. It is possible to observe that the results obtained from the Gaussian distribution (squares) approaches the theoretical (solid line) and the computational (points) results obtained from the waterbag distribution. In this way, it is possible to conclude that even using a different initial momentum distribution from the theoretical model, the flow behavior and electric field at the cathode are almost the same. Moreover, Fig. 3.3(a) shows the abrupt transition between the accelerate and the

[2] As it will be shown in subsection 3.1.5, this is not always true.

space charge limited regime is still occurring when the Gaussian distribution is used. It indicates that the results from the waterbag distribution can be extended, and, Fig. 3.3(b) shows that even changing the parameters (increasing injection temperature), there is still having a good approximation of the results.

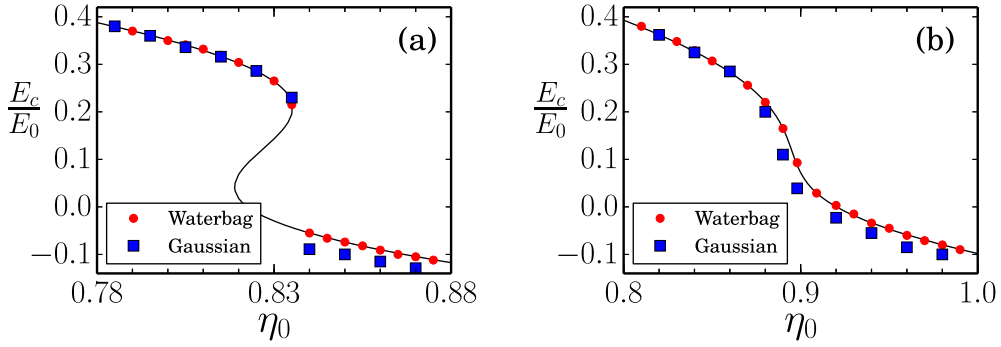

Fig. 3.3: Normalized electric field at cathode as function of the charge intensity for (a) $T_0 = 8.33 \times 10^{-4}$ and (b) $T_0 = 3.33 \times 10^{-3}$– the same parameters used in Fig. 3.1. The solid line corresponds to results from the theory whereas the symbols from the simulation with waterbag (points) and Gaussian (squares) initial momentum distributions. In this figure is observed that results from a waterbag and a Gaussian are similar.

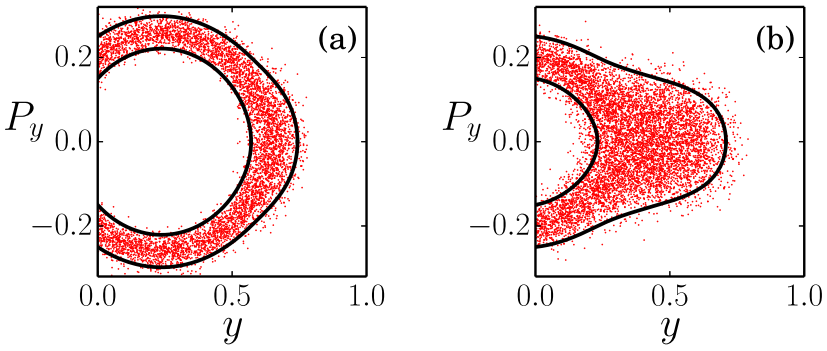

Fig. 3.4: Phase space plots before (a) and after (b) the abrupt regime transition showed in Fig. 3.3(a) when the Gaussian distribution is used. These figures indicate that the dramatic change in charge distribution presented in Fig. 3.2 occurs even for a different initial momentum distribution.

The phase space for a Gaussian distribution of the electron before (a) and after (b) the abrupt transition presented in Fig. 3.3(a) are show in Fig. 3.4. There, solid lines represent theoretical solution for the most and the least energetic electron of the flow (waterbag distribution) and dots

represent the particle position obtained from simulation (Gaussian distribution). It is possible to observe the theoretical solution describes the collective behavior of the flow before and after the phase transition.

3.1.3 The critical temperature

The results introduced up to now show that when the initial electron temperature is relatively small, the transition between accelerate and space charge limited is abrupt. In contrast, when the initial electron temperature is relatively large, the transition between accelerate and space charge limited is continuous. It indicates that there is a critical injection temperature T_{0c} which separates the occurrence of the abrupt and the continuous regime transition. In order to confirm that really exists such critical injection temperature and to find its value, the phase-diagram η_0 vs. T_0 was constructed and presented in Fig. 3.5. In the phase-diagram, for a determined injection temperature, the dashed line defines where the transition is continuous while the solid line defines where the regime transition is abrupt. The critical temperature that separates those regimes is represented by the point and its value is $T_{0c} \approx 1.4 \times 10^{-3}$. The region between the solid and the dotted line corresponds to the region where multiple stationary solutions are found.

It is worth noting that the results presented in Fig. 3.5 are from theory assuming the initial momentum distribution is a waterbag distribution. However, as discussed in subsection 3.1.2, these results can be extended to the Gaussian initial momentum distribution resulting the same characteristics.

3.1.4 The stationary state when $P_{0min} \to 0$

The smallest momentum that an electron must have to be emitted from the cathode is $P_{0min} = 0$. It defines the higher injection temperature of the flow[3] $T_{0max} \equiv T_0^* = \bar{P}_0^2/3$ or, from Eq. (2.48), $T_0^* = T_{0max}/12$. When the injection temperature is such as $T_0 \to T_0^*$, another interesting dynamical feature emerges. This is illustrated in Figs. 3.6 and 3.7, constructed assuming the following parameters:

[3]Although the temperatures T_0 and T_0^* have the same physical meaning, they define two different systems, such as, whenever T_0^* is used, it is assumed $P_{0min} = 0$.

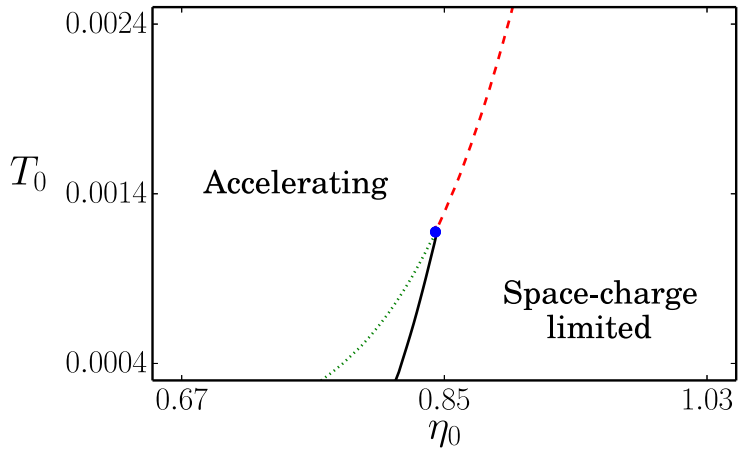

Fig. 3.5: Phase-diagram η_0 vs. T_0 showing where the transition between accelerating and space charge limited regime is continuous (dashed line) or abrupt (solid line). The point represents the critical temperature T_{0c} that separates those regimes. The multiple stationary solutions are found in the region between the solid and the dotted line.

$\nu_0 = 0.8$ (MI mode), $\eta_0 = 0.6$, $\bar{P}_0 = 0.2$ and $T_0^* = 1.33 \times 10^{-2}$. For this parameter set, Eq. (2.56) with the boundary conditions predicts a single stationary solution with $E_c/E_0 = 0.645$. In order to verify this result, Fig. 3.6 was made. There, the time evolution of $E_c(t)/E_0$ obtained from the $N-$particle simulation (solid line) is presented. When the electrons start entering the gap region between the cathode and the anode, the $E_c(t)/E_0$ value decrease from the unity until the expected theoretical value (dashed line). However, at longer times ($t \sim 10^3$), the $E_c(t)/E_0$ value decrease again until the electron flow achieves a new laminar and stable stationary solution with $E_c(t)/E_0 \approx 0.37$.

To clarify what is happening, snapshots of the phase space obtained at different times are shown in Fig. 3.7. While for $t = 10^2$ (a), the borders of the $N-$particle simulation agree with the theory, for $t = 2 \times 10^3$ (b) some particles start populating the region inside $P_y(P_{0min}, y)$. This occurs because the charges that enter in the system with vanishingly small momentum almost follow the $P_y(P_{0min}, y)$ curve in phase space. In the absence of any perturbation they would return to the cathode and reach it with a correspondingly small momentum. However, due to oscillations in the electron distribution, some of these particles loose energy while traversing the system, becoming unable to reach back the cathode. In other words, those particles stay trapped inside the gap region. This

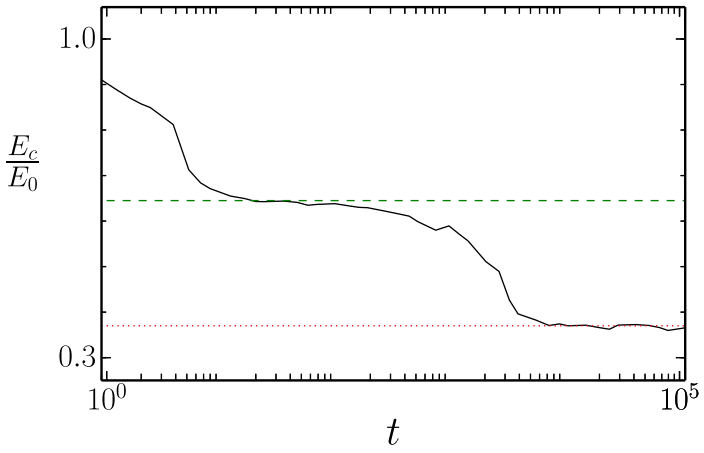

Fig. 3.6: Time evolution of the normalized electric field measured over the cathode. The solid line is the result obtained from the particle simulation while the dashed and the dotted lines are results predicted from theory. The parameters used here were: $\nu_0 = 0.8$ (MI mode), $\bar{P}_0 = 0.2$ and $T_0^* = 1.33 \times 10^{-2}$.

process continues on and on, building progressively more charge in the system. It only ceases when the region inside $P_y(P_{0min}, y)$ is completely filled with the maximum density allowed by the Vlasov equation. Thereafter, the particles stop being trapped and the flow becomes laminar again.

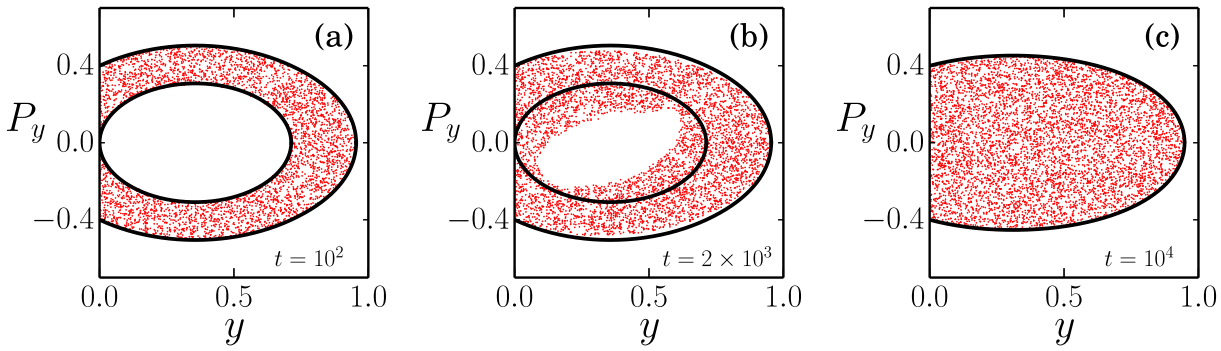

Fig. 3.7: Phase space obtained at different instants of time. Thick black lines correspond to the charge distribution boundaries predicted by the theory while dots are the particle position in phase space obtained from simulation when (a) $t = 10^2$, (b) $t = 2 \times 10^3$ and (c) $t = 10^4$. In order to compare, the parameters used here are the same as used in Fig. 3.6.

Hence, the particle density of the *final* stationary state is given by Eq. (2.38) supposing $P_y(P_{0min}, y) = 0$ (this can be observed in Fig. 3.7(c)). Replacing this result in the Poisson equation (2.30), the fol-

lowing differential equation for the scalar potential is obtained:

$$\frac{\partial^2\phi}{\partial y^2} = 2\eta_0 \frac{|\sqrt{P_{0max}^2 - y^2 + \nu_0\phi(y)}|}{P_{0max}}. \tag{3.3}$$

The Eq. (3.3) is subject to the boundaries $\phi(0) = 0$ and $\phi(1) = 1$. Now, solving Eq. (3.3) using the same parameters of Fig. 3.6, the *final* stationary state predicted by theory is $E_c(t)/E_0 = 0.371$ (dotted line in Fig. 3.6) and the corresponding $P_y(P_{0max}, y)$ curve is shown in Fig. 3.7(c). Both results clearly agree with the simulation. This process that destabilizes the stationary state of Fig. 3.7(a) is similar to the phenomena discussed in Refs. [9, 34] in the context of a cold electron flow. The main difference is that there the instability is driven by external agents and leads to the onset of a near-Brillouin flow [34], whereas, here it is driven by intrinsic oscillations of the electron distribution and the final state (Fig. 3.7(c)) is an accelerating regime.

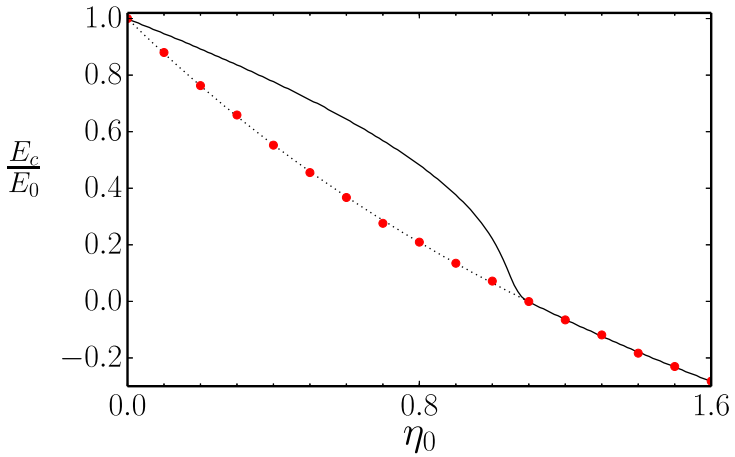

Fig. 3.8: Normalized electric field at the cathode for the stationary state as function of the charge intensity η_0. The parameters used here are: $\nu_0 = 0.8$ (magnetic insulation mode), $\bar{P}_0 = 0.2$ and $T_0^* = 1.33 \times 10^{-2}$. The solid line is the result obtained from the theory when the curve $P_y(P_{0min}, y)$ is taken into account and the dashed line is the result obtained from the theory when the curve $P_y(P_{0min}, y)$ is considered null. Points are the results from particle simulation.

The results from simulation for the normalized electric field over the cathode at the stationary state as a function of the charge intensity using the parameters $\nu_0 = 0.8$ (magnetic insulation mode), $\bar{P}_0 = 0.2$ and $T_0^* = 1.33 \times 10^{-2}$ are shown in Fig. 3.8. There, the solid line is the theoretical solution

when the curve $P_y(P_{0min}, y)$ is taken into account and the dashed line is the theoretical solution when the curve $P_y(P_{0min}, y)$ is *not* taken into account. The results from simulation show that the dashed solution is the *true* solution branch. Since the cathode can emit electrons with momentum varying from zero to some finite velocity, the stationary solution with $T_0 = T_0^*$ is the most likely to be observed experimentally.

3.1.5 Stationary to nonstationary transition

Although Fig. 3.2(b) shows that the electron flow at space charge limited regime is stationary and laminar for a finite injection temperature and charge intensity, it stops being true when the injection temperature goes to zero (cold case) and the charge intensity is large enough. However, analyzing the stationary solutions and discovering to which injection temperature and charge intensity the electron flow is stationary or nonstationary (turbulent) is a difficult task. It happens because the linear stability theory might *not* be useful to determine the occurrence of turbulence since the system starts far from the stationary solution and might never reach it to be perturbed[4]. Then, in order to circumvent this difficulty, a detailed nonlinear analysis of the electron dynamics in the gap was performed to determine when the system is more or less robust against fluctuations.

To proceed with the nonlinear analysis, it was assumed that the flow was emitted with the maximum allowed temperature ($T_0 = T_0^*$). As discussed in subsection 3.1.4, the electron flow under this condition is driven to a single steady state solution region where the charge density is described by Eq. (2.38) assuming $P_y(P_{0mim}, y) = 0$.

Supposing the phase space trajectory (Eq. (2.54)) of the most energetic electron emitted from the cathode ($P_y(P_{max}, y) \equiv P_{ymax}$) and taking the second derivative with respect to time, the following differential equation is obtained[5]:

[4]The initial condition occurs with the gap empty and the stationary solution occurs when the gap is filled by electrons in the allowed region.

[5]In order to obtain Eq. (3.4) these mathematical relations were used: $\dot{P}_{ymax} = (\partial P_{ymax}/\partial y)(\partial y/\partial t) = (\nu_0/2)(\partial\phi/\partial y) - y$, $\ddot{P}_{ymax} = P_{ymax}(\partial\dot{P}_{ymax}/\partial y)$, and $\partial^2\phi/\partial y^2 = \eta_0|P_{ymax}|/P_{0max}$, where $\partial y/\partial t = P_{max}$.

$$\ddot{P}_{ymax} + \left(1 - \frac{\nu_0\eta_0}{P_{0max}}\left|P_{ymax}\right|\right) P_{ymax} = 0, \tag{3.4}$$

subject to the boundary conditions $P_{ymax}(0) = P_{0max}$ and $\dot{P}_{ymax}(0) = -\nu_0 E_c/2$. Eq. (3.4) is equivalent to Llewellyn form [9, 35] for a thermal crossed field gap. Differently from the cold case, this equation is nonlinear and does *not* have a simple solution. However, even without finding an explicit solution, important properties of the particle trajectory are possible to get just constructing an effective potential for its momentum evolution. Multiplying Eq. (3.4) by $2\dot{P}_{max}/P_{0max}^2$ and integrating it in relation to the time, it is found that:

$$\mathcal{K}(\dot{P}_{ymax}) + \mathcal{V}(P_{ymax}) = \mathcal{E} \tag{3.5}$$

where,

$$\mathcal{K}(\dot{P}_{ymax}) \equiv \frac{\dot{P}_{ymax}^2}{P_{0max}^2} \tag{3.6}$$

is an effective kinetic energy,

$$\mathcal{V}(P_{ymax}) \equiv \left(1 - \frac{2\nu_0\eta_0}{3}\left|\frac{P_{ymax}}{P_{0max}}\right|\right)\left(\frac{P_{ymax}}{P_{0max}}\right)^2 \tag{3.7}$$

is the effective potential that drives the dynamic of P_{ymax}, and

$$\mathcal{E} \equiv \frac{\nu_0^2 E_c^2}{4P_{0max}^2} + 1 - \frac{2\nu_0\eta_0}{3} \tag{3.8}$$

is an integration constant that acts like an effective energy for the trajectory. To evaluate it, the boundary conditions $P_{ymax}(0) = P_{0max}$ and $\dot{P}_{ymax}(0) = -\nu_0 E_c/2$ were applied in Eq. (3.5).

The shape of the effective potential $\mathcal{V}$ is shown by the thick solid curve in Fig. 3.9 for the choice of parameters $\nu_0\eta_0 = 1.5$ (a) and $\nu_0\eta_0 = 0.95$ (b). Both cases present a local minimum at $P_{ymax} = 0$. To the parameters of panel (a) there is also two symmetric maximums. From Eq. (3.7), it is observed

that the maximums are located at $P_{ymax} = \pm f_p$ with $f_p = P_{0max}/\nu_0\eta_0$. The maximums are absent from panel (b) because for that case $\mid P_{0max} \mid < \mid f_p \mid$. In the figure is also presented the straight line that represents the value of the effective energy for $T_0^* = 0.0075$. To the trajectories shown, the particle is injected with P_{0max} and starts decreasing its momentum (moving to the left in the figure) because $\dot{P}_{ymax} < 0$ at the cathode (space charge limited case). Since $\mathcal{E} > \mathcal{V}$ for all P_{ymax} there are *not* turning points where $\dot{P}_{ymax}$ changes its sign (see Eq. (3.5)). Hence, P_{ymax} continuously decrease until the particle reaches the cathode again with a momentum $-P_{0max}$ and leaves the system.

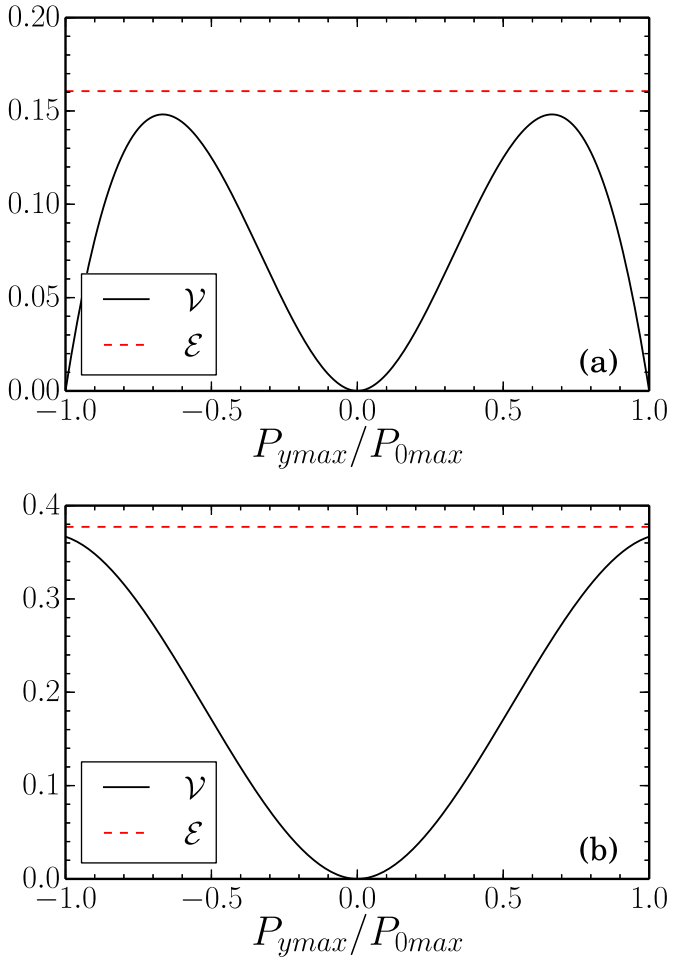

Fig. 3.9: Plots of the effective potential (solid curve) for $\nu_0\eta_0 = 1.5$ (a) and $\nu_0\eta_0 = 0.95$ (b). The dashed lines show the corresponding values of the energy for $T_0^* = 0.0075$.

In practice, however, as the system relaxes it presents fluctuations that will cause both $\mathcal{E}$ and $\mathcal{V}$ to

vary in time. If at a certain instant of time $\mathcal{E} = \mathcal{V}$, there will be a change in the sign of $\dot{P}_{ymax}$ and the particle momentum will start bouncing inside the effective potential well, which may prevent the system from reaching the time independent stationary state. It is expected the smaller is the difference between the theoretically predicted values of $\mathcal{E}$ and $\mathcal{V}$, the more likely is such an event. Then, the following parameter was defined:

$$\Delta = \min[\mathcal{E} - \mathcal{V}(P_{ymax})], \tag{3.9}$$

here the minimization is to be taken along the stationary solution trajectory $-P_{0max} \leq P_{ymax} \leq P_{0max}$. The smallness of Δ is foreseen to serve as an indicator of how sensitive the stationary solution is to the fluctuations. From Fig. 3.9(a) is clear that when $\nu_0\eta_0 > 1$ and the maximums of the effective potential are present that $\Delta = \min[\mathcal{E} - \mathcal{V}(f_p)]$. On the other hand, when $\nu_0\eta_0 < 1$, such as in Fig. 3.9(b), the minimization in Eq. (3.9) leads to $\Delta = \min[\mathcal{E} - \mathcal{V}(P_{0max})]$. To perform a qualitative analysis of the parameter space where the system is more sensitive to fluctuations, a region where Δ is smaller than a chosen critical value Δ_c was determined. This corresponds to the colored area in Fig. 3.10. Since the solid line marks the transition between accelerating (left) and space charge limited regime (right), it is possible to conclude that in a small region near to the regime transition, the electron flow is sensitive to fluctuations. Moreover, from the theoretical curve is observed that $\Delta(\eta_0, T_0^*) = \Delta_c = 0.02$ (dashed line), keeping the injection temperature constant and increasing the charge intensity or keeping the charge intensity constant[6] and decreasing the injection temperature, the flow become more and more sensitive to fluctuations.

The evolution of the total force ($F_e(y_f) = -\nu_0 E(y_f)/2 - y_f$) acting upon a test particle fixed at $y_f = 0.35$ as obtained from simulations assuming the parameters $\nu_0 = 0.8$, $\eta_0 = 3.0$ (space charge limited regime), and two different values of T_0^* is plotted in Fig. 3.11. There, it is observed that for both injection temperatures the force undergoes violent oscillations in the beginning. However, for the higher T_0^* case (dashed curve), it eventually saturates to a nearly constant value indicating that the

[6]The charge intensity must be large enough to set the flow at the space charge regime.

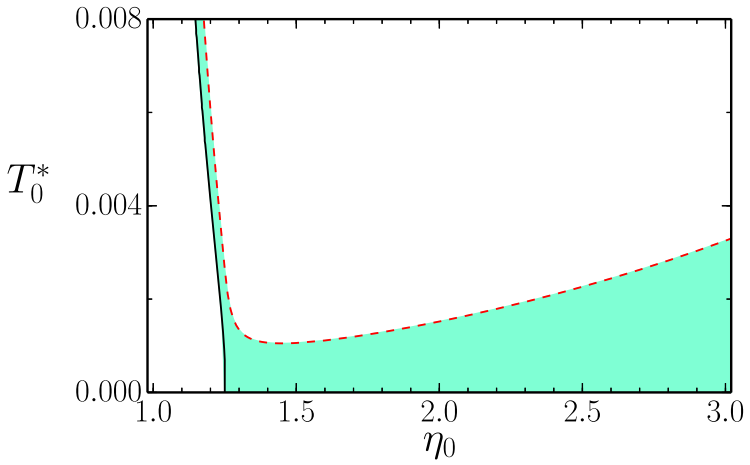

Fig. 3.10: Parameter space of η_0 vs. T_0^*. The solid curve corresponds to the points where the cathode electric field vanishes, $E_c = 0$, and marks the transition between accelerating (smaller η_0) and space charge limited (larger η_0) regimes. The dashed curve shows the points where $\Delta(\eta_0, T_0^*) = \Delta_c$, with $\Delta_c = 0.02$. The colored region represents the points where $0 \leq \Delta \leq \Delta_c$

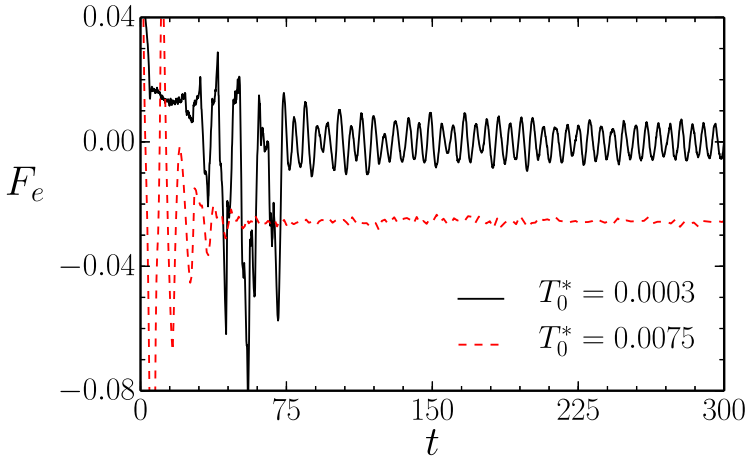

Fig. 3.11: Time evolution of the effective force acting on a test particle at $y = 0.35$ as obtained from self-consistent simulations in the space charge limited regime. For $T_0^* = 0.0075$ (dashed curve) the force eventually reaches a stationary value that agrees with the theoretically predicted one, whereas for $T_0^* = 0.0003$ (solid curve) the force shows persistent oscillations. The other parameters are $\eta_0 = 3.0$ and $\nu_0 = 0.8$.

system has reached the stationary state. In fact, the stationary value of the total force at $y_f = 0.35$ calculated from the theory is $F_e = -0.0255$ which is in excellent agreement with the one obtained in

the simulation. Note that the total force is negative because in the space charge limited stationary state all the particles are pushed back towards the cathode. The F_e value has been evaluated at different positions and they all relax to constant values that match with the theoretically predicted ones. On the other hand, for the lower temperature (solid curve) the solution presents persistent oscillations around zero that do not fade and prevent the system from attaining the stationary state. These oscillations are clearly related to the changes in the sign of P_{ymax} as discussed. Based on the results of Fig. 3.11, it is possible to conclude that the turbulent state is characterized by the occurrence of a positive total force acting upon the particles after the initial transient time.

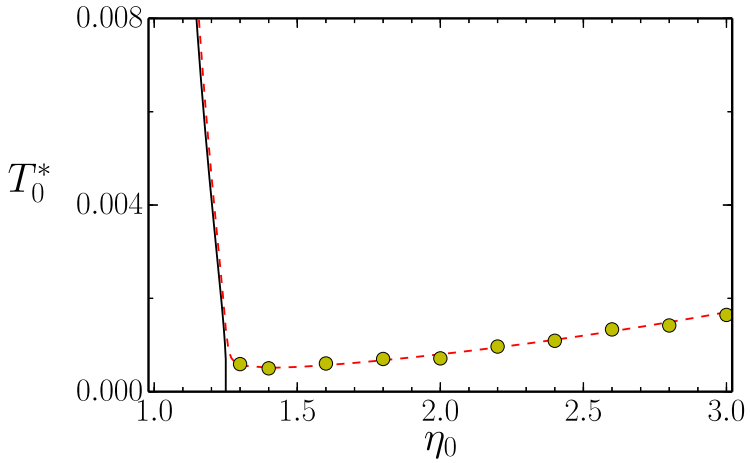

Fig. 3.12: Parameter space η_0 vs. T_0^*. The symbols show the injection temperature above which the system attains a time- independent stationary state in the self-consistent simulations for the given η_0. The dashed curve corresponds to the theoretical curve $\Delta(\eta_0, T_0^*) = \Delta_c$ obtained with $\Delta_c = 0.006$. The solid curve marks the transition between accelerating (left) and space charge limited regimes (right).

Hence, in order to determine when the stationary to the nonstationary transition occurs, computational simulations for times longer than the transient time were run. In the simulations, the injection temperature was increased from 0 at small increments until the condition $F_e < 0$ was found for all the particles, indicating that a time-independent stationary regime has emerged. The results obtained for different values of η_0 are shown in Fig. 3.12, where the symbols represent the injection temperature above which the system attains the time-independent stationary state. To test the theoretical results

obtained from the effective potential analysis, the Δ_c that best fits the numerical results was searched. It was observed that the theoretical curve obtained using the value $\Delta_c = 0.006$ (dashed curve) fits with a good accuracy the results of the simulation. Because the nonstationary region near the accelerating to the space charge limited regime is very small to large temperatures, the $N-$particles simulations were not accurate enough to prove that.

It is important to note that, although Fig. 3.12 is showing that there is *no* stationary states for temperatures below $T_0^* \approx 0.003$, in conflict with the results of Fig. 3.5, it is *not* possible to compare directly those, since they represent different problems. While the phase space region inside the curve $P_y(P_{0max}, y)$ is empty for the case represented in Fig. 3.5, it is completely filled for the case represented in Fig. 3.12. Moreover, the average momentum of the electrons entering the gap is very different in each case. While it is large in the case shown in Fig. 3.5, it goes to zero in the case shown in Fig. 3.12 and, when the average momentum is quite small, the fluctuations become more evident. Then, just to clarify, the results presented in Fig. 3.5 are in a true stationary state.

3.2 Nonrelativistic Child-Langmuir and no-cutoff modes

In this section, both the Child-Langmuir and the no-cutoff modes are analyzed in the nonrelativistic limit. When the electron flow is at the stationary mode CL, all electrons emitted from the cathode reach the anode after a transient time and the charge density as function of y is given by Eq. (2.41). Then, in this mode, the scalar potential is given by the following equation:

$$\frac{\partial^2 \phi}{\partial y^2} = \eta_0 \frac{|\sqrt{P_{0max}^2 - y^2 + \nu_0 \phi(y)}| - |\sqrt{P_{0min}^2 - y^2 + \nu_0 \phi(y)}|}{P_{0max} - P_{0min}}, \tag{3.10}$$

subject to the boundaries $\phi(0) = 0$ and $\phi(1) = 1$. Using $\zeta_0 = 0$ and Eq. (2.54) in Eq. (2.40), it is possible to observe that the CL mode occurs when:

$$\nu_0 > 1 - P_{0min}^2. \tag{3.11}$$

The CL condition (3.11) is still valid until the charge density become large enough to the electron flow be at space charge limited regime. When it happens, the slower electrons can *no longer* reach the anode. However, because there are still electrons reaching the anode, the electron flow is at no-cutoff mode and the particle density is given by Eq. (2.44). To the NC mode, the scalar potential equation is given by:

$$\frac{\partial^2\phi}{\partial y^2} = 2\eta_0 \frac{|P_y(P_{0lim}, y)| - |P_y(P_{0min}, y)|}{P_{0max} - P_{0min}} + \eta_0 \frac{|P_y(P_{0max}, y)| - |P_y(P_{0lim}, y)|}{P_{0max} - P_{0min}}, \tag{3.12}$$

where P_{0lim} is given by Eq. (2.43). Eq. (3.12) must satisfy the boundary conditions $\phi(0) = 0$ and $\phi(1) = 1$.

The results from the theory (solid and dotted lines) and from the simulation (points) for the normalized electric field E_c/E_0 as a function of the charge intensity using the parameters $\nu_0 = 1.2$ (supposedly at CL mode), $\bar{P}_0 = 0.2$ and $T_0 = 8.33 \times 10^{-4}$ are shown in Fig. 3.13(a). From the simulation results, it can be observed that when $\eta_0 = 2.90 \rightarrow 2.91$, the normalized electric E_c/E_0 value changes from $E_c/E_0 = 0$ to $E_c/E_0 = -0.4$. Analyzing the electron flow phase space before (Fig. 3.14(a)) and after (Fig. 3.14(b)) that abrupt change in the E_c/E_0 value, it is observed that there is an abrupt regime transition from accelerated to space charge limited and there is a mode transition from CL to NC. Thus, in Fig. 3.13(a), the solid line is the theoretical solution supposing the flow is at the CL mode and the particle density is given by (2.41) and the dotted line is the theoretical solution supposing the flow is at the NC mode and the particle density is given by Eq. (2.44). All the results were verified by the $N-$particle simulation. As it is possible to conclude, there is a good agreement between the results from theory and from simulation. Whereas in Fig. 3.14(a) the flow is described by $P(P_{0min}, y)$ and $P(P_{0max}, y)$ curves, in Fig. 3.14(b) the flow is described by $P(P_{0min}, y)$, $P(P_{0lim}, y)$, and $P(P_{0max}, y)$ curves. Note, the curve $P(P_{0lim}, y)$ is segmented in order to represent the electrons which reach the anode and the electrons which return to the cathode.

The results from the theory (solid and dotted lines) and from the simulation (points) for the nor-

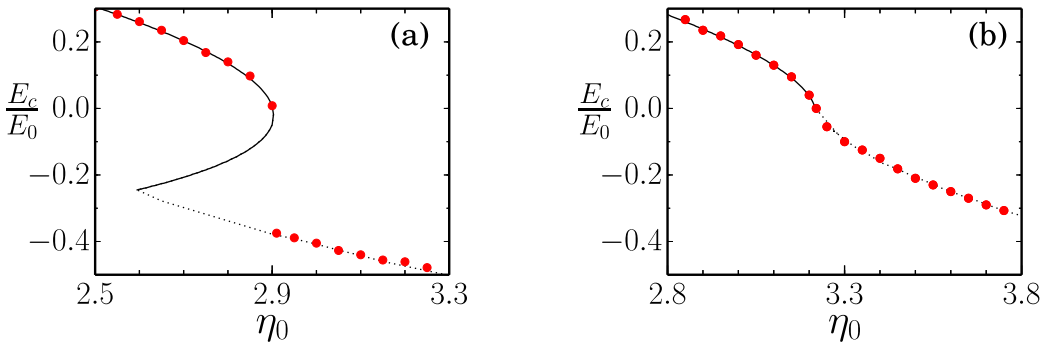

Fig. 3.13: Normalized electric field at the cathode for the stationary state as function of the charge intensity η_0 for (a) $T_0 = 8.33 \times 10^{-4}$ and (b) $T_0^* = 1.33 \times 10^{-2}$. The solid and the dotted lines correspond to the results from the theory supposing the CL and the NC mode, respectively, whereas the symbols are the results of the simulation. Accelerating and space charge limited regime correspond to $E_c/E_0 > 0$ and $E_c/E_0 < 0$, respectively. Other parameters are $\nu_0 = 1.2$ (supposedly at Child-Langmuir mode) and $\bar{P}_0 = 0.2$.

malized electric field E_c/E_0 as a function of the charge intensity when parameters are the same used in Fig. 3.13(a), except $T_0 = T_0^* = 1.33 \times 10^{-2}$, are shown in Fig. 3.13(b). From the simulation results, it can be observed that when $\eta_0 = 3.2$, there is a continuous regime transition from accelerated to space charge limited and there is a mode transition from CL to NC mode. When $\eta_0 < 3.2$, the theoretical solutions are obtained supposing the flow is at the CL mode (solid line) and the particle density is given by Eq. (2.41). On the other hand, when $\eta_0 > 3.2$, the theoretical solutions are obtained supposing the flow is at the NC mode (dotted line) and the particle density is given by Eq. (2.44). All the results were verified by the $N-$particle simulation. As it is possible to observe, there is a good agreement between the results from theory and simulation and the mode transition CL to NC really occurs. Observing that, when $P_{0min} \to 0$ the electric field to decelerate the flow is such as $E_c \to 0$, it follows that only when $T_0 = T_0^*$ (it means $P_{0min} = 0$), the mode transition CL to NC is continuous.

When $1 - P_{0max}^2 < \nu_0 \leq 1 - P_{0min}^2$, the electron flow is at the NC mode and the scalar potential Eq. (3.12) with boundary conditions allows to describe the electron flow in the gap and to evaluate E_c/E_0. It is worth noting that the NC mode only occurs when there is a momentum spread ($T_0 \neq 0$) around an average electron momentum.

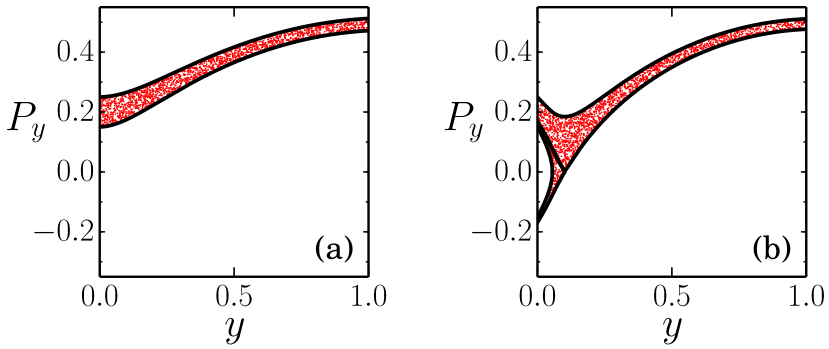

Fig. 3.14: Phase space plots of the electron flow at the stationary state. The solid lines in (a) are the curves $P_y(P_{0min}, y)$ and $P_y(P_{0max}, y)$, and the solid lines in (b) are the curves $P_y(P_{0min}, y)$, $P_y(P_{0lim}, y)$, and $P_y(P_{0max}, y)$ obtained from the theory. The dots (simulation) represent the electron position in phase space. Specifically, the figures show the abrupt transition identified in Fig. 3.13(a). When the charge intensity is increased from (a) $\eta_0 = 2.90$ to (b) $\eta_0 = 2.91$, the electron flow changes mode (CL to NC) and regime (accelerating to space charge limited).

The values obtained for E_c/E_0 as function of the charge intensity using the parameters $\nu_0 = 0.96$, $\bar{P}_0 = 0.2$ and $T_0 = 3.33 \times 10^{-3}$ are shown in Fig. 3.15(a). There, the solid lines represent the results from theory while the points represent the normalized electric field obtained from simulation. The value of ν_0 was chosen such that the electrons emitted from the cathode with $P_0 = \bar{P}_0$ reach the anode with zero momentum. In analogy to previous cases, it may be noted that as the charge intensity in the system is increased, the electric field value on the cathode decreases. Specifically, when $\eta_0 = 1.39 \rightarrow 1.40$ the electron flow regime changes from accelerate ($E_c/E_0 = 0.30$) to space charge limited ($E_c/E_0 = -0.20$). Again, it can be observed that the values of E_c/E_0 obtained from simulation and theory agree with good accuracy.

The electron phase space before (a) and after (b) the regime transition identified in Fig. 3.15(a) is show in Fig. 3.16. The dots represent the particle position, obtained from the simulation and the solid lines represent curves $P_y(P_{0min}, y)$, $P_y(P_{0lim}, y)$, and $P_y(P_{0max}, y)$ obtained from theory.

In Fig. 3.17, the particle evolution on the phase space assuming the parameters $\nu_0 = 0.96$, $\bar{P}_0 = 0.2$, $\eta_0 = 1.0$ and $T_0^* = 1.33 \times 10^{-2}$ is shown. Because $T_0 \rightarrow T_0^*$ the particles evolve in the phase space through a similar process discussed in section 3.1.4. All the electrons of the flow can gain our lose energy because the charge distribution oscillations. Those electrons emitted from the

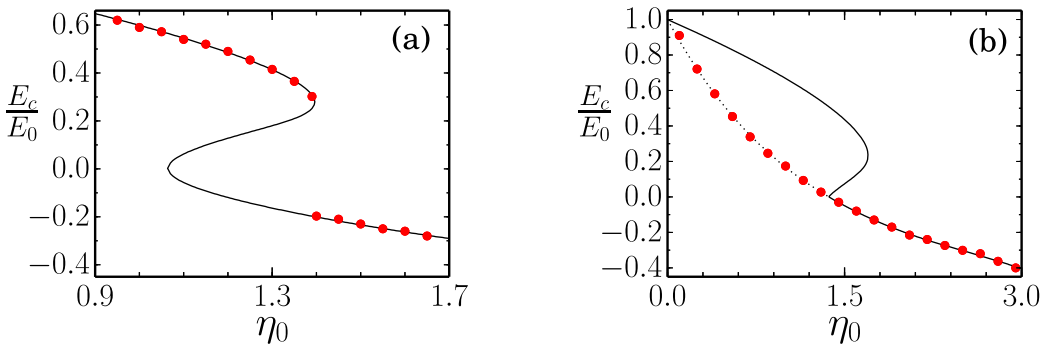

Fig. 3.15: Normalized electric field at the cathode for the stationary state as function of the charge intensity η_0 for (a) $T_0 = 3.33 \times 10^{-4}$ and (b) $T_0^* = 1.33 \times 10^{-2}$. The solid line corresponds to results from the theory when the curve $P_y(P_{0min}, y)$ is taken into account and the dotted line is the result obtained from the theory when the curve $P_y(P_{0min}, y)$ is considered null. The symbols are the results from the simulation. Accelerating and space charge limited regimes correspond to $E_c/E_0 > 0$ and $E_c/E_0 < 0$, respectively. Other parameters are $\nu_0 = 0.96$ (no cutoff mode) and $\bar{P}_0 = 0.2$.

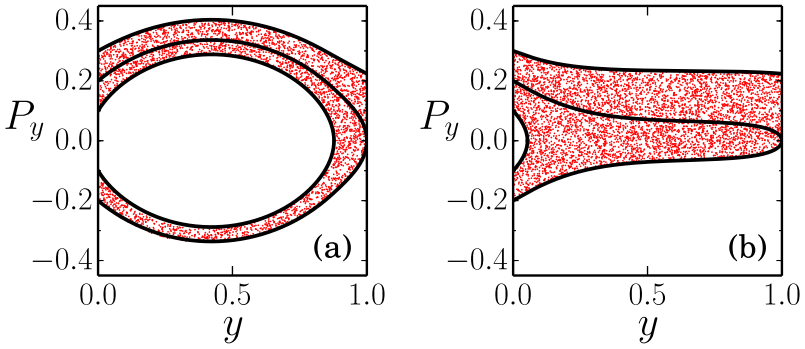

Fig. 3.16: Phase space plots of the stationary state. Dots are the particle position in phase space obtained from simulation after the flow became stationary and thick black lines correspond to the charge distribution boundaries predicted by the theory. A slight increase in the charge intensity from (a) $\eta_0 = 1.39$ to (b) $\eta_0 = 1.40$ drives the regime from the accelerating to the space charge limited, producing a dramatic change in the charge distribution.

cathode with small momentum $P_{0min} \to 0$ that lose energy might be trapped in the gap region not returning to the cathode. At the time instant $t = 50$ (a) the curves $P_y(P_{0min}, y)$, $P_y(P_{0lim}, y)$, and $P_y(P_{0max}, y)$, obtained from the theory, describe the distribution bounds. However, when $t = 300$ (b) the distribution begins to populate the inner region of the curve $P_y(P_{0min}, y)$ and finally, when $t = 5000$ (c) the distribution reaches a new steady state. Therefore, solving the scalar potential Eq. (3.3) with the boundary conditions is the correct way to treat the electrons confined in the gap

($P_{0mim} \leq P_0 < P_{0lim}$). With this result, it is possible to conclude that the NC mode is really a composition of the MI and the NC mode and the phenomena observed in the MI case does also occur in the NC case.

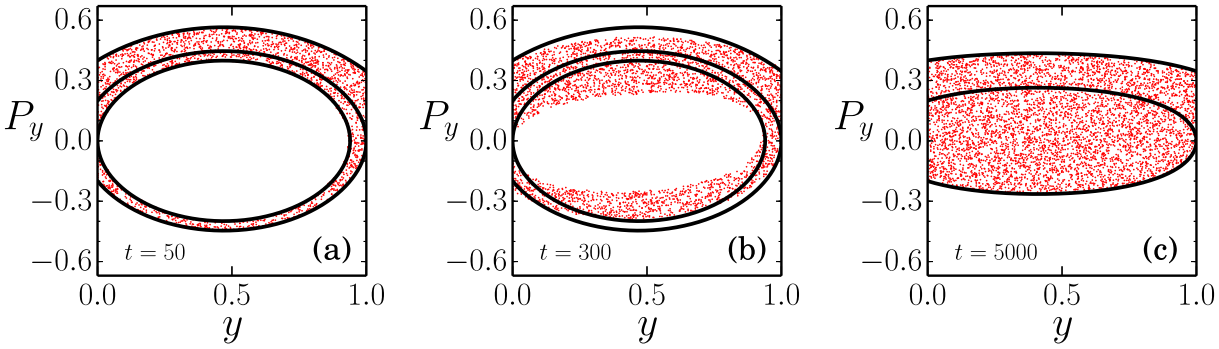

Fig. 3.17: Phase space at different instants of time. The solid lines are the results obtained from the theory whereas the dots are from simulation. It can be concluded from the simulation that the flow is driven to a new steady state obtained from theory assuming $P_y(P_{0min}, y) = 0$. Here, $\nu_0 = 0.96$, $\eta_0 = 1.0$, $T_0^* = 1.33 \times 10^{-2}$, and $\bar{P}_0 = 0.2$.

In Fig. 3.15(b), the E_c/E_0 value as function of the charge intensity using the parameters $\nu_0 = 0.96$ (NC mode), $\bar{P}_0 = 0.2$ and $T_0^* = 1.33 \times 10^{-2}$ is shown. There, the points represent the normalized values obtained from the simulation while the solid (dotted) line represents the theoretical solution when the curve $P_y(P_{0min}, y)$ is (*not*) taken into account.

3.3 Relativistic regime

In the relativistic approach, to describe the electron flow, the scalar and the vector potential must be evaluated together. Thus, to obtain the theoretical solutions, it is necessary to solve self-consistently Eqs. (2.30) and (2.34) with their boundary conditions[7]. Once these potentials are determined, from the relativistic Hamiltonian Eq. (2.25) is possible to get information of each electron in the gap. Additionally, to obtain the computational results, it is necessary to solve Eqs. (2.49) and

[7]Since the Hamiltonian was used to determine the particle density, implicitly it is solved with the electromagnetic potentials.

(2.50) where the electric field is given by Eq. (2.51) and the vector potential and the magnetic field are obtained using an electrostatic particle in the cell (PIC) method.

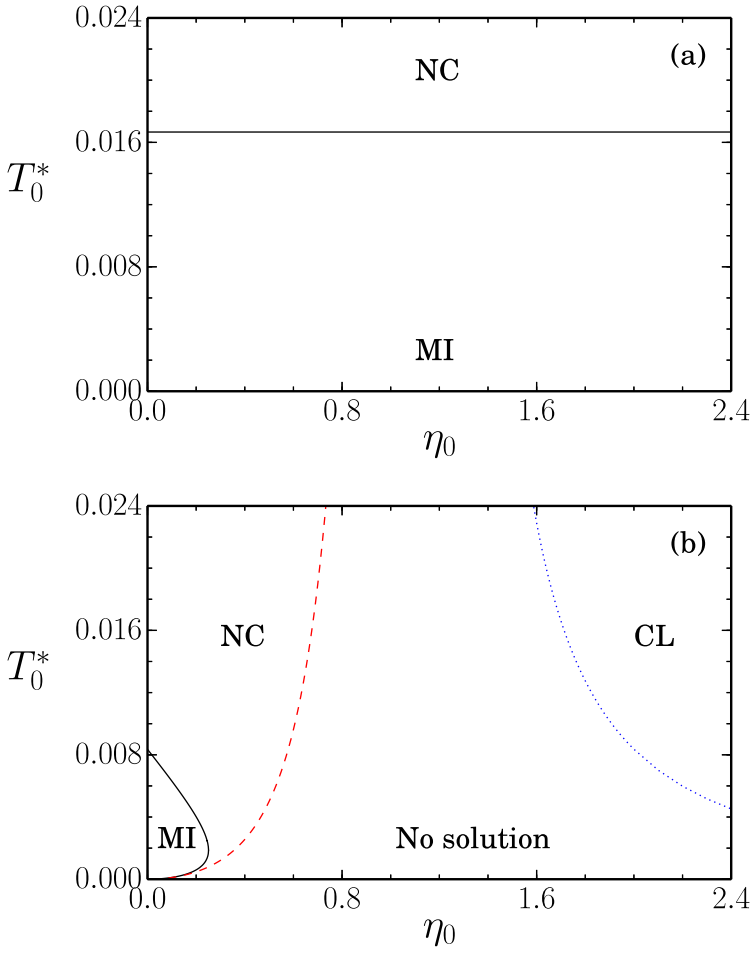

Fig. 3.18: Parameter space of η_0 vs. T_0^*. These figures show the parameter regions where each stationary mode is found supposing $\nu_0 = 0.8$. It can be observed that when $\zeta_0 = 0.00001$ and the flow is nonrelativistic (a) the mode transition MI to NC occurs to a theoretical injection temperature $T_0^* \approx 0.016$. On the other hand, when $\zeta_0 = 0.2$ and the flow is relativistic (b), the parameter regions where each stationary mode is found become completely different. Then, changing the injection temperature or the charge intensity, the electron flow can change to different stationary modes. In addition, it is possible to observe a large region where there is no theoretical solution predicted by the theory developed here.

Since in the relativistic approach the self-magnetic field is taken into account, it is not possible to know what is the vector potential at the anode ($A_x(y = 1)$) and then, it is not possible to determine *a priory* which is the stationary state of the flow. This difficulty is evidenced at the parameter space

of η_0 vs. T_0^* presented in Fig. 3.18. It was made to show that setting $\nu_0 = 0.8$ and changing the ζ_0 parameter, going from the nonrelativistic limit ($\zeta_0 = 0.00001$) to the slightly relativistic case ($\zeta_0 = 0.2$), the parameter regions where each stationary mode occur is strongly modified. In the nonrelativistic case presented in Fig. 3.18(a), two distinct parameter regions corresponding to the MI or the NC stationary mode are observed. Thus, for example, when the injection temperature is lower than 0.016, regardless of the charge intensity, the flow is at the stationary state MI. In contrast, when the injection temperature is higher than 0.016, the flow is at the stationary state NC. Theoretically, it is possible to obtain from the relation (3.1) that the transition between the MI and the NC mode occurs when $T_0^* = 0.0166$, regardless of the charge intensity. Furthermore, from relation (3.11), it is possible to conclude when $\nu_0 = 0.8$ the transition between the NC and the CL mode is not possible, independently of the injection temperature.

In contrast to the results of the nonrelativistic case, when the flow is slightly relativistic ($\zeta_0 = 0.2$), as shown in Fig. 3.18(b), the mode transitions happens in different parameter regions. This because now the transitions between the modes are determined by Eqs. (2.40) and (2.42) which depend on the vector potential value over the anode. The potential vector changes according to the charge intensity in the gap, and then, when the charge intensity is modified, the steady state of the flow is also modified. Physically, the electrons moving in the gap generate a self-magnetic field that decreases the magnetic shielding, making them get closer or reach the anode. Another characteristic observed in Fig. 3.18(b) is that there is a region where no theoretical solutions are found using the waterbag model developed here. However, that region can be accessed using the $N-$particle simulation (see Fig. 3.22).

In Fig. 3.19, the phase space plots of the electron flow at the stationary state setting $\nu_0 = 0.8$, $\zeta_0 = 0.2$, and $\eta_0 = 0.22$ and varying the injection temperature is shown. When $T_0^* = 0.006 \rightarrow 0.001875$, the electron flow changes from the NC mode (a) to the MI mode (b). From the classical equations is expected that setting the parameters and decreasing the injection temperature, the flow became more confinable (see Fig. 3.19(a)). However, it is possible to note that for a lower temperature, such as $T_0^* = 0.0006$, the flow is at NC mode again (c) and that is completely unexpected. This result shows that for small injection temperatures, the electron flow may not be confined.

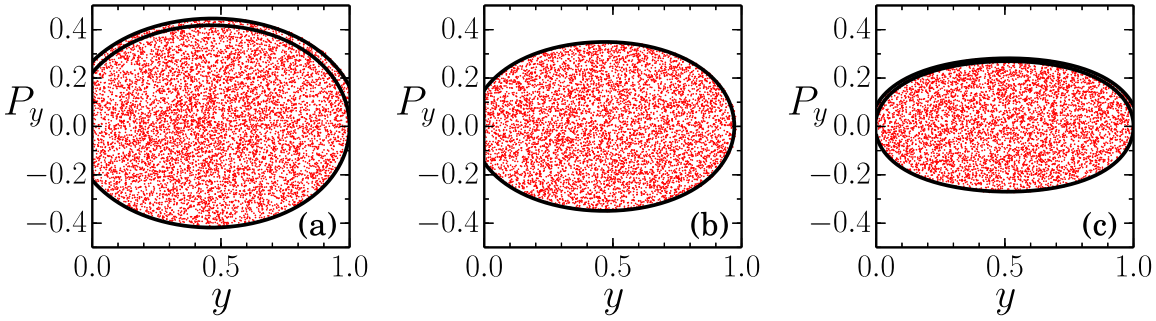

Fig. 3.19: Phase space plots of the stationary state. Dots are the particle position in phase space obtained from simulation after the flow became stationary and thick black lines correspond to the charge distribution boundaries predicted by the relativistic approach. When the charge intensity is kept constant and the injection temperature is decreased from $T_0^* = 0.006$ to $T_0^* = 0.001875$, the electron stationary flow changes from the NC (a) to the MI mode (b). This type of behavior was expected by the nonrelativistic approach. However, reducing even more the injection temperature until $T_0^* = 0.0006$, the flow changes to the NC mode (c) and it was not expected. Here: $\nu_0 = 0.8$ and $\eta_0 = 0.22$.

In addition, in Fig. 3.20 the phase space plots of the electron flow at the stationary state setting $\nu_0 = 0.8$, $\zeta_0 = 0.2$, and $T_0^* = 0.006$ and varying the charge intensity is shown. When the charge intensity is small such as $\eta_0 = 0.01$, a solution that corresponds to the MI mode is found and presented in Fig. 3.20(a). Increasing the charge intensity until $\eta_0 = 0.22$, it is observed the flow changes to the NC mode (see Fig. 3.19(a)) and, increasing even more the charge intensity until $\eta_0 = 2.4$, it is found that the flow is at the CL mode, as shown in Fig. 3.20(b).

It is important to note when the charge intensity goes to zero, the injection temperature to promote the transition between the MI and the NC mode presented in Fig. 3.18(b) should be the same for the relativistic and the nonrelativistic case. However due to the normalization used here, increasing the relativistic parameter results in increasing the canonical momentum and thus, even when $\eta_0 = 0$, the injection temperature to the mode transition is different. Moreover, it appears the mode transitions are promoted by the self-magnetic field, since using the classical equations and the self-magnetic field the mode transitions are still occurring.

Therefore, although variations produced by the self-magnetic field are small, they are enough to

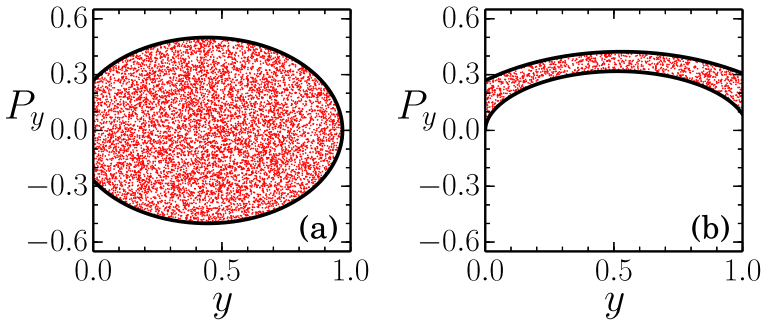

Fig. 3.20: Phase space plots of the stationary state. Dots are the particle position in phase space obtained from simulation after the flow became stationary and thick black lines correspond to the charge distribution boundaries predicted by the relativistic approach. Setting the injection temperature and increasing the charge intensity from $\eta_0 = 0.01$ to $\eta_0 = 2.4$, the flow changes from the MI (a) to the CL mode (b). Here: $\nu_0 = 0.8$ and $T_0^* = 0.006$.

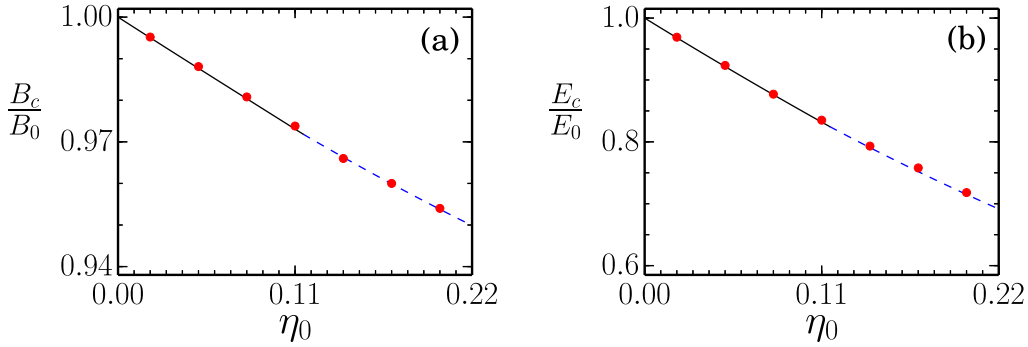

Fig. 3.21: Normalized magnetic field (a) and normalized electric field (b) at the cathode for the stationary state as function of the charge intensity for $T_0^* = 0.006$ and $\nu_0 = 0.8$. The solid line was obtained from the theory supposing the magnetic insulated mode, and the dotted line was obtained from the theory supposing the no-cutoff mode. The symbols are the results obtained from the $N-$ particle simulation.

promote the mode transitions. In Fig. 3.18(b) the smaller magnetic field value is such as: $B_c/B_0 = 0.9$. It means that a variation of 10% in the magnetic field is enough to the transitions showed in Fig. 3.18(b) occur. To clarify, Fig. 3.21 shows how the magnetic field (a) and the electric field (b) changes as the charge intensity is increased and $T_0^* = 0.006$ and $\nu_0 = 0.8$. To those parameters, the theoretical transition MI (solid line) to NC (dotted line) does occur when $\eta_0 = 0.113$. It means in that case a variation of 3% in the magnetic field promoted the mode transition. These results were verified by

the $N-$particle simulation (symbols).

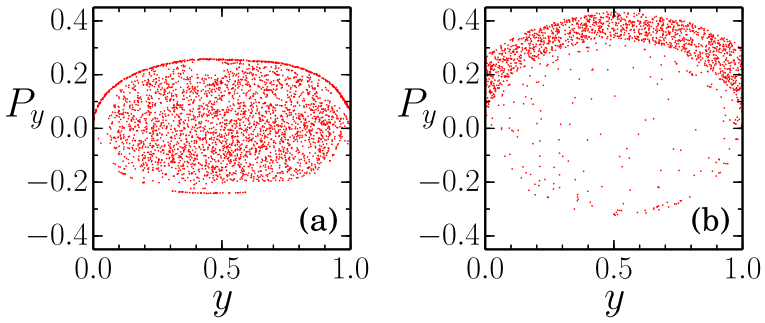

Fig. 3.22: Phase space plots at the no solution region showed in Fig. 3.18. Dots are the particle position in phase space after a long transient of time. The figure (a) shows that particles are partially confined when the particle density is $\eta_0 = 0.22$ and the injection temperature goes to zero ($T_0^* = 0.000133$). The figure (b) shows that when $\eta_0 = 1.5$ and $T_0^* = 0.006$ the particles are partially confined and the flow presents two different densities.

Finally, Fig. 3.22 shows two phase space plots of the electron flow corresponding to the "no solution"region of Fig. 3.18(b). When the charge intensity is $\eta_0 = 0.22$ and injection temperature goes to zero ($T_0^* = 0.000133$), the flow is partially confined, as evidenced in Fig. 3.22(a) but that could not be the final stationary state since that system configuration is very sensitive. Therefore, the limit $T_0^* \to 0$ needs to be more investigated in order to confirm if in the no solution region the flow is really at the NC mode when the maximum injection temperature is equal to zero[8]. When $\eta_0 = 1.5$ and $T_0^* = 0.006$, the electron flow is partially confined and the existence of two densities stands out why the theoretical solutions were not found in that region as is shown in 3.22(b).

[8]The simulations become complicated in the limit $T_0^* \to 0$ because the electron density goes to infinity.

Chapter 4

Conclusions

In this thesis, a mathematical model to describe the electron flow in a crossed electromagnetic field configuration was presented. Specifically, the stationary states of an electron flow subjected to the fields observed in a smooth-bore magnetron was analyzed. From the theoretical and the computational results, it was possible to understand how the system parameters (average initial momentum, injection temperature, electron density in the gap, and potential difference between the cathode and the anode) change the stationary states of the electron distribution.

Among the many results obtained, it was observed that in the nonrelativistic magnetic insulated (MI) mode, when the electron injection temperature went to zero, the transition between the accelerating to the space charge limited regime was abrupt[1]. The abrupt transition disappeaed when the electron injection temperature was increased, indicating there was a critical temperature that separates both regimes. The critical temperature was found through a parameter map. As it was shown, those results could be found by using a more complex initial momentum distribution, like a Gaussian. Moreover, it was verified, when the electrons were *not* pre-accelerated entering the gap, the *final* stationary state was modified due to charge oscillations. In a special condition, when the injection temperature went to zero and the charge intensity was large enough to drive the flow to the space

[1] It means increasing a little bit the charge intensity, the stationary state is modified changing from the accelerating to the space charge limited regime.

charge limited regime, the electron flow has not achieved the stationary state and only a turbulent solution was found. The turbulent solution occurrence was because particles trapped in the gap. Then, the transition between the laminar and the turbulent flow was characterized by different parameters.

Analyzing the nonrelativistic Child-Langmuir (CL) mode, it was observed the regime transition (accelerating to space charge limited) occurred together with the mode transition Child-Langmuir to no-cutoff. Those transitions were always abrupt except when there were electrons being emitted from the cathode with zero velocity. As it was shown, the no-cutoff mode was a composition of the magnetic insulated and the Child-Langmuir mode.

Studying the relativistic limit, both electric and magnetic self-fields were taken into account. This because even small the self-magnetic field could promote mode transitions which were not foreseen when only the self-electric field was taken into account. Through these results, a better understanding and controlling of the experimental results is expected to be achieved.

As a next step to develop the theoretical electron flow description in the crossed field configuration, it is necessary to verify what happens at the low temperature and charge intensity limit when the relativistic parameter goes to zero, it is also desirable to investigate the "no solution"region using a two (or more) charge density model to verify if it is possible to get theoretical solutions in that region. Moreover, to evolve and validate this work is necessary to confirm experimentally all these theoretical results.

Appendix A

Green's functions

In this appendix it is presented how Green's functions are used to solve analytically the Poisson equation (2.30) satisfying the boundary conditions (2.31) and (2.32).

A.1 Scalar potential solution

In computer simulation discussed in section 2.3, N particles generate a self-consistent potential $\phi_s(y)$- observe that the scalar potential $\phi(y)$ is composed by self-consistent $\phi_s(y)$ and the external potential $\phi_0(y)$. Each charge in gap region produces a small perturbation in the electric potential; it is assumed these perturbations are Dirac delta functions in geometric space; thus the Green's function indicates the weight of these Dirac delta functions must have for the scalar potential differential equation be satisfied with its contours [30].

Let an inhomogeneous differential equation (2.30) with boundaries (2.31) and (2.32); whether there is solution for the differential equation:

$$\nabla^2 G(y, s) = \delta(y - s), \tag{A.1}$$

satisfying Dirichlet boundary conditions:

$$G(y=0,s)=0 \tag{A.2}$$

and

$$G(y=1,s)=0, \tag{A.3}$$

where $G(y,s)$ is a Green function, s is the position where the Dirac delta functions are measured (it is the particles position in the geometric space) and $\delta(y-s)$ is the Dirac delta function, such that: $\delta(y-s)=0$ if $y\neq s$ and $\delta(y-s)\to\infty$ if $y=s$; then, the scalar potential solution $\phi(y)$ is given by:

$$\phi(y)=\eta_0\int G(y,s)n(s)ds+\phi_0(y). \tag{A.4}$$

Note that, boundary conditions (A.2) and (A.3) are equal to zero because the particles can not change the potential over both the anode and the cathode. The differential equation (A.1) with boundaries (A.2) and (A.3) can be solved resulting in the following Green's function:

$$G(y,s)=\begin{cases}(s-1)y & \text{if} \quad y<s,\\ (y-1)s & \text{if} \quad y\geq s.\end{cases} \tag{A.5}$$

From (A.4) and (A.5), the scalar potential can be written as:

$$\phi(y)=\eta_0\int_0^y s(y-1)n(s)ds+\int_y^1 y(s-1)\eta_0 n(s)ds+y. \tag{A.6}$$

Observing the particle density is $n(s)=\sum_{j=1}^{N}\frac{\delta(s-s_j)}{N}$; equation (A.6) can be written as:

$$\phi(y)=y\left(1+\frac{\eta_0}{N}\sum_{j=1}^{N}\int_0^1 s\delta\left(s-s_j\right)ds-\frac{\eta_0}{N}\sum_{j=1}^{N}\int_y^1\delta\left(s-s_j\right)ds\right)-\frac{\eta_0}{N}\sum_{j=1}^{N}\int_0^y s\delta\left(s-s_j\right)ds. \tag{A.7}$$

Solving the integrals in equation (A.7), it is obtained:

$$\phi_i(y) = y\left(1 + \frac{\eta_0}{N}\sum_{j=1}^{N} s_j - \frac{\eta_0}{N}\sum_{j=i+1}^{N} 1\right) - \frac{\eta_0}{N}\sum_{j=1}^{i+1} s_j. \tag{A.8}$$

Defining $\bar{y} \equiv \frac{1}{N}\sum_{j=1}^{N} s_j$ as the average position of the particles, $\bar{y}_l^i \equiv \frac{1}{N}\sum_{j=1}^{i+1} s_j$ as the average position of the particle below the particle i and $n_r^i \equiv \sum_{j=i+1}^{N} 1$ as the number of particles above the particle i plus one, it is found:

$$\phi_i(y) = y\left(1 + \eta_0\bar{y} - \eta_0\frac{n_r^i}{N}\right) - \eta_0\bar{y}_l^i. \tag{A.9}$$

From equation (A.9) and relation (2.12), it is observed the electric field in the gap region is:

$$E_y^i = -\left(1 + \eta_0\bar{y} - \eta_0\frac{n_r^i}{N}\right). \tag{A.10}$$

Equation (A.10) is the same presented in (2.51).

References

[1] L. Robert. *The magnetron*. Chapman & Hall, 1952.

[2] A. S. Gilmour. *Klystrons, traveling wave tubes, magnetrons, cross-field ampliers, and gyrotrons*. Artech House, 2011.

[3] D. M. Goebel; and I. Katz. *Fundamentals of Electric Propulsion: Ion and Hall Thrusters*. John Wiley & Sons, Inc, 2008.

[4] J. Andersson; and A. Anders. Self-sputtering far above the runaway threshold: An extraordinary metal-ion generator. *Phys. Rev. Lett.*, 102:045003, 2009.

[5] C. D. Child. Discharge from hot CaO. *Phys. Rev. (Series I)*, 32:492, 1911.

[6] A. W. Hull. The effect of a uniform magnetic field on the motion of electrons between coaxial cylinders. *Phys. Rev.*, 18:31, 1921.

[7] I. Langmuir. The effect of space charge and initial velocities on the potential distribution and thermionic current between parallel plane electrodes. *Phys. Rev.*, 21:419, 1923.

[8] R. C. Davidson; and H. S. Uhm. Kinetic stability properties of nonrelativistic non-neutral electron flow in a planar diode with applied magnetic field. *Phys. Rev. A*, 32:3554, 1985.

[9] Y. Y. Lau; P. J. Christenson; and D. Chernin. Limiting current in a crossed-field gap. *Phys. Fluids B*, 5:4486, 1993.

[10] Y. Y. Lau; J. W. Luginsland; K. L. Cartwright; D. H. Simon; W. Tang; B. W. Hoff; and R. M. Gilgenbach. A re−examination of the Buneman−Hartree condition in a cylindrical smooth-bore relativistic magnetron. *Phys. Plasmas*, 17:033102, 2010.

[11] D. J. Kaup. Theoretical modeling of crossed-field electron vacuum devices. *Phys. Plasmas*, 8:2473, 2001.

[12] G. H. Goedecke; B. T. Davis; C. Chen; and C. V. Baker. On steady flows in smooth-walled magnetrons: Fundamental modes and no-cutoff flows in planar geometry. *Phys. Plasmas*, 12:113104, 2005.

[13] G. H. Goedecke; B. T. Davis; and C. Chen. Magnetic insulation at finite temperatures. *Phys. Plasmas*, 13:083104, 2006.

[14] R. C. Davidson; H.-W. Chan; C. Chen; and S. Lund. Equilibrium and stability properties of intense non-neutral electron flow. *Rev. Mod. Phys.*, 63:341, 1991.

[15] P. J. Christenson; and Y. Y. Lau. Transition to turbulence in a crossed-field gap. *Phys. Plasmas*, 1:3725, 1994.

[16] M. Lopez; Y. Y. Lau; J. W. Luginsland; D. W. Jordan; and R. M. Gilgenbach. Limiting current in a relativistic diode under the condition of magnetic insulation. *Phys. Plasmas*, 10:4489, 2003.

[17] Y. Y. Lau; J. W. Luginsland; K. L. Cartwright; and M. D. Haworth. Role of ions in a crossed-field diode. *Phys. Rev. Lett.*, 98:015002, 2007.

[18] P. Zhang; and Y. Y. Lau. Ultrafast strong-field photoelectron emission from biased metal surfaces: exact solution to time-dependent Schrödinger equation. *Sci. Rep.*, 6:19894, 2016.

[19] S. Marini; F. B. Rizzato; and R. Pakter. Thermal effects and space-charge limited transition in crossed-field devices. *Phys. Plasmas*, 21:083111, 2014.

[20] S. Marini; R. Pakter; and F. B. Rizzato. Transition to space-charge limited flow in crossed-field devices. *MOPWA002 in Proceedings of IPAC2015*, 2015.

[21] S. Marini; F. B. Rizzato; and R. Pakter. Stationary to nonstationary transition in crossed-field devices. *Phys. Plasmas*, 23:033107, 2016.

[22] D. J. Kaup. *Future Directions of Nonlinear Dynamics in Physical and Biological Systems*. Plenum Press, 1993.

[23] R. C. Davidson. *Physics of Nonneutral Plasmas*. World Scientific Publishing Company; 2^a ed., 2001.

[24] F. B. Rizzato; R. Pakter; and Y. Levin. Driven one-component plasmas. *Phys. Rev. E*, 80:021109, 2009.

[25] E. Peter; A. Endler; F. B. Rizzato; and A. Serbeto. Mixing and space-charge effects in free-electron lasers. *Phys. Plasmas*, 20:123104, 2013.

[26] J. D. Jackson. *Classical electrodynamics*. John Wiley & Sons Inc, 3^a ed., 1998.

[27] Y. Levin; R. Pakter; and T. N. Teles. Collisionless relaxation in non-neutral plasmas. *Phys. Rev. Lett.*, 100:040604, 2008.

[28] T. N. Teles; R. Pakter; and Y. Levin. Relaxation and emittance growth of a thermal charged-particle beam. *App. Phys. Lett.*, 95:173501, 2009.

[29] W. H. Press. *Numerical Recipes in FORTRAN Example Book: The Art of Scientific Computing*. Cambridge University Press, 1992.

[30] E. Butkov. *Mathematical Physics*. Addison-Wesley, 1^a ed., 1968.

[31] C. K. Birdsall; and A. B. Langdon. *Plasma Physics via Computer Simulation*. Taylor & Francis, 1991.

[32] A. Antoniazzi; D. Fanelli; S. Ruffo; and Y. Y. Yamaguchi. Nonequilibrium tricritical point in a system with long-range interactions. *Phys. Rev. Lett.*, 99:040601, 2007.

[33] R. Pakter; and Y. Levin. Core-halo distribution in the hamiltonian mean-field model. *Phys. Rev. Lett.*, 106:200603, 2011.

[34] P. J. Christenson; D. P. Chernin; A. L. Garner; and Y. Y. Lau. Resistive destabilization of cycloidal electron flow and universality of (near-) Brillouin flow in a crossed-field gap. *Phys. Plasmas*, 3:4455, 1996.

[35] C. K. Birdsall; and W. B. Bridges. *Electron Dynamics of Diode Regions*. Academic, 1966.